An Enhanced SPEI Drought Monitoring Method Integrating Land Surface Characteristics

Liqing Peng[1*], Justin Sheffield[2], Zhongwang Wei[3], Michael Ek[4], Eric F. Wood[5†]

[1] Food Program, World Resources Institute, Washington DC, United States.
[2] School of Geography and Environmental Science, University of Southampton, Southampton, United Kingdom.
[3] Southern Marine Science and Engineering Guangdong Laboratory (Zhuhai), Guangdong Province Key Laboratory for Climate Change and Natural Disaster Studies, School of Atmospheric Sciences, Sun Yat-Sen University, Guangzhou, China.
[4] Joint Numerical Testbed, Research Applications Laboratory, National Center for Atmospheric Research, Boulder, Colorado, United States.
[5] Department of Civil and Environmental Engineering, Princeton University, Princeton, New Jersey, United States. (†Deceased)

***Correspondence to*:** Liqing Peng (pengliqing51@gmail.com)

Abstract. Atmospheric evaporative demand is a key metric for monitoring agricultural drought. The existing ways of estimating evaporative demand in drought indices do not faithfully represent the constraints of land surface characteristics and become less accurate over non-uniform land surfaces. This study proposes incorporating surface vegetation characteristics, such as vegetation dynamics data, aerodynamic and physiological parameters, into existing potential evapotranspiration (PET) methods. This approach is implemented over the Continental United States (CONUS) for the period of 1981-2017 and is tested in a recently developed drought index the Standardized Precipitation Evapotranspiration Index (SPEI). We show that activating realistic maximum surface and aerodynamic conductance could improve prediction of soil moisture dynamics and drought impacts by 29% on average compared to the widely used simple methods, especially effective in the forests and humid regions. Surface characteristics that have a strong influence on the performance of the SPEI are mainly driven by leaf area index (LAI). Our approach only requires the minimum amount of ancillary data, while permitting both historical reconstruction and real-time forecast of drought. This offers a physically meaningful, yet easy-to-implement way to account for the vegetation control in drought indices.

1 Introduction

Drought is one of the most costly hydrological hazards (Wilhite, 2000; Ross & Lott, 2003; Piao et al., 2019), with devastating impacts on croplands and pastures (Kogan, 1995), forests ecosystems (Clark et al., 2016; Xu et al., 2022), electricity production, water quality, and soil fertility (Loon, 2015). Monitoring the changes in water availability is critical for providing early warnings of drought and for risk management (Wilhite, Sivakumar, & Pulwarty, 2014). Many physical or probabilistic measures have been developed (Heim, 2002) to quantify drought, such as Palmer Drought Severity Index (PDSI, Palmer, 1965), Standardized Precipitation Index (SPI, McKee, Doesken, Kleist, & others, 1993), Vegetation Condition Index (VCI, Kogan, 1995), and multiple remote sensing drought indices (Zhang, Jiao, Zhang, Huang, & Tong, 2017; Yang et al., 2023).

Atmospheric evaporative demand (AED) is a key input to drought indices because it is a measure of water demand, namely, how thirsty the atmosphere is (Peng, Li, & Sheffield, 2018). AED typically reflects the effect of temperature and humidity, and is considered a major driver of drought stress on vegetation and tree mortality (Williams et al., 2012; McDowell et al., 2018). Among the drought indices, the recently developed Standardized Precipitation Evapotranspiration Index (SPEI) (Vicente-Serrano, Beguería, & López-Moreno, 2010) factors in water demand (AED) in addition to water supply (precipitation). Compared to the SPI that only considers precipitation, the SPEI is more suitable for quantifying the drought impacts on agriculture (Potop, 2011; Potop, Možný, & Soukup, 2012), and ecosystems (Vicente-Serrano et al., 2012; Vicente-Serrano et al., 2013; Barbeta, Ogaya, & Peñuelas, 2013). In addition, the SPEI is more flexible than the PDSI because it is not sensitive to soil water field capacity and can be implemented on various time scales (Vicente-Serrano, der Schrier, Beguería, Azorin-Molina, & Lopez-Moreno, 2015; Zhao et al., 2017). It has been widely used for both drought reconstruction and monitoring (Paulo, Rosa, & Pereira, 2012; Beguería, Vicente-Serrano, Reig, & Latorre, 2013).

The way of estimating AED in drought indices has a significant impact on drought quantification (Sheffield, Wood, & Roderick, 2012; Trenberth et al., 2013; Yang, Roderick, Zhang, McVicar, & Donohue, 2018; Dewes et al., 2017). AED is approximated by potential evapotranspiration (PET), the maximum rate of evapotranspiration when surface water supply is unlimited. Previous work has used various PET formulations for AED in the SPEI since it was first proposed in 2010 (Vicente-Serrano, Beguería, & López-Moreno, 2010; Beguería, Vicente-Serrano, Reig, & Latorre, 2013). These conventional PET methods do not factor in the effects of surface characteristics, which often assume no or simple universal vegetation control on transpiration (e.g., the Thornthwaite, Hargreaves-Samani, and Penman methods). Without vegetation control, the maximum surface conductance is overestimated and the PET rate during the onset and retreat of the growing season is unrealistically high. Furthermore, by assuming an smooth reference surface, some methods

Deleted: The

Deleted: on transpiration is often neglected

Deleted: and therefore

do not account for surface roughness, hence downplay aerodynamic conductance and suppress the PET estimate (Peng et al., 2019). Even though the reference evapotranspiration (ET_0) method (Allen, Pereira, Raes, & Smith, 1998) considers the biophysical limitation of transpiration by assigning a surface resistance under well-watered condition, it does not account for vegetation phenology (Lorenz, Davin, Lawrence, Stöckli, & Seneviratne, 2013) and assumes a fixed reference height and a constant surface resistance for all vegetation types. This approach is not physically meaningful for forests, where canopy height is relatively large and vegetation cover varies significantly. A recent study by Sun et al. (2023) highlighted the importance of incorporating surface properties especially vegetation control in PET and used a two source model designed for sparse vegetation surfaces. However, the model's broader applicability beyond sparse vegetation is uncertain, and additionally it may increase data requirements and associated uncertainties.

We hypothesize that adding the surface vegetation characteristics to an existing drought quantification approach will improve the spatial and temporal accuracy of drought prediction. The goals of this study are to explore which surface features are the most useful for enhancing drought prediction, and which vegetation types benefit most from incorporating these features. We propose incorporating realistic vegetation restrictions into existing PET methods, while not increasing much cost and uncertainty caused by additional data sources and complex formulations. Then we use independent soil moisture observations (Dai, Trenberth, & Qian, 2004) from satellite to evaluate the drought depictions by various forms of PET approaches across different temporal scales. The evaluation against observed soil moisture allows the direct diagnosis of the most sensitive surface characteristics and the most effective approach for drought quantification (Vicente-Serrano et al., 2012).

In this study, we focus on the continental U.S. (CONUS) primarily because the drought events hitting this region have raised interest in variability, trends, and future risks of drought (Andreadis & Lettenmaier, 2006; Hobbins et al., 2012; Dewes et al., 2017). Several most severe droughts hit the western U.S. in the recent decade, including the 2012 Great Plains drought (Hoerling et al., 2014) and the 2012-2016 California drought (Dong et al., 2019). The western U.S. has been experiencing the most severe drought period after the 1930s and 1950s (Andreadis, Clark, Wood, Hamlet, & Lettenmaier, 2005), and its vulnerability to drought continued to grow (Andreadis & Lettenmaier, 2006). Besides, high-quality meteorological datasets are available over the CONUS (Daly et al., 2008; Xia et al., 2012) and can help reduce the uncertainty of drought prediction originating from input forcings.

2 Data

2.1 Meteorology

To calculate the SPEI, PET is estimated on daily scale over the period of 1981-2017 using high-quality daily meteorology data from PRISM (Parameter-elevation Regressions on Independent Slopes Model) that employs weather stations and digital elevation model (Daly, Neilson, & Phillips, 1994; Daly et al., 2008). We acquire daily precipitation, daily mean, maximum, minimum, and dew point temperature on a 4 km grid for the period of 1981-2017. Surface downward shortwave and net longwave radiation, pressure, and wind speed are taken from the NLDAS-2 (North American Land Data Assimilation System phase 2 (Xia et al., 2012). All data are spatially restricted to the continental United States (25–50^{o}N, 67–125^{o}W) and regridded to the 0.125^{o} NLDAS-2 grid using the first-order conservative remapping tool provided by Climate Data Operators (https://code.zmaw.de/projects/cdo).

2.2 Soil moisture

The European Space Agency Climate Change Initiative (ESA CCI) v4.3 surface soil moisture (SMsurf) is used to evaluate the drought severity quantified by the SPEI time series (https://www.esa-soilmoisture-cci.org/). This dataset combines several active and passive microwave soil moisture products into a harmonized surface layer soil moisture (2-5 cm) in m^3 m^{-3} (Liu et al., 2012; Gruber et al., 2017). The dataset is chosen for its enhanced data reliability by integrating multiple single-sensor active and passive microwave soil moisture products to minimize uncertainty (Gruber et al., 2019). The version 4.3 provides soil moisture on a 0.25^{o} grid at daily time step for the 1979-2017 period and has been widely used in ET and drought studies (Dorigo et al., 2017; Martens et al., 2017).

2.3 Land surface ancillary data

The land surface data used for deriving biophysical parameters include gridded land cover type, leaf area index, and surface albedo. The land cover type is provided by the 0.5 km MODIS-based Global Land Cover Climatology during the 2001-2010 period (Broxton, Zeng, Sulla-Menashe, & Troch, 2014, https://archive.usgs.gov/archive/sites/landcover.usgs.gov/global_climatology.html). This dataset has 17 land cover classes based on the International Geosphere - Biosphere Program (IGBP) classification. This land cover climatology dataset is displayed in Fig. 1.

The monthly climatology of leaf area index is obtained from the 15-day, 1 km AVHRR GIMMS LAI3g product that covers the period of 1982-2016 (Zhu et al., 2013). The monthly climatology of surface albedo is derived from the 8-day, 0.05^{o} GLASS (Global Land Surface Satellite) albedo product. This

Deleted: we

Deleted: e

GLASS02A05/06 product combines MODIS and AVHRR (Advanced Very-High-Resolution Radiometer) to provide a gap-filled land surface shortwave black-sky and white-sky albedo (Qu et al., 2014; Liu et al., 2013) that covers the period of 1982-2012. We resample the 8-day albedo to a daily resolution and obtain daily albedo by averaging the black- and white-sky albedos. Missing data are gap-filled using the average of adjacent years.

The canopy height data are obtained from a global tree height dataset at 1-km for 2005 using spaceborne lidar (Simard et al., 2011).

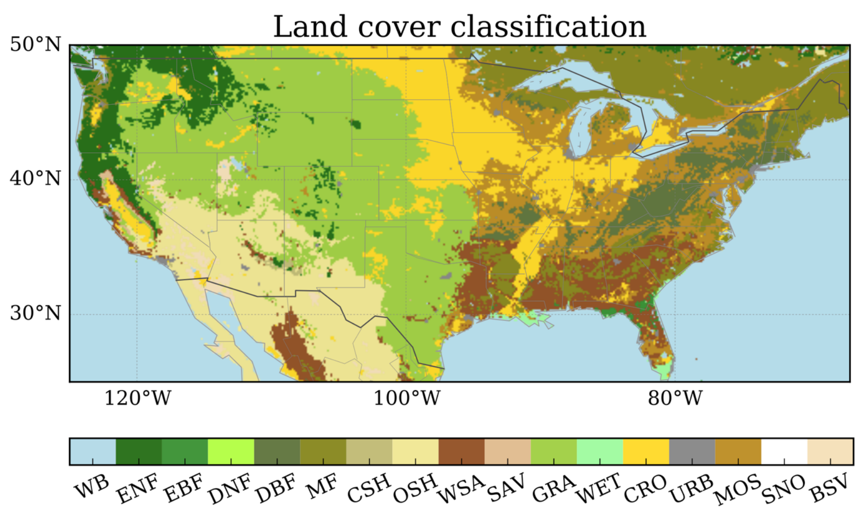

Figure 1. The land cover classification over the Continental United States used for surface vegetation parameter inference. The classification is based on the satellite retrieval of land cover climatology during 2001-2010 (see Table 1 for a list of land cover full names).

3 PET methods

3.1 Current PET methods

PET can be estimated from univariate empirical models such as temperature-based methods (Thornthwaite, 1948) and physically-based models. Empirically based methods can induce large uncertainty in the drought projection (Sheffield et al., 2012; Feng, Trnka, Hayes, & Zhang, 2017) and are therefore not considered in the study. Physically-based methods can account for multiple input variables such as surface net radiation,

Moved (insertion) [2]

near-surface temperature, wind speed, or specific humidity. The Penman equation (Penman, 1948) is the most comprehensive physically-based method to estimate PET by combining the radiative and aerodynamic components:

$$PET_{Penman} = \frac{\Delta(R_n - G) + \rho_a C_p D Ga}{\lambda(\Delta + \gamma)} \qquad (1)$$

where PET is expressed as water mass fluxes (kg m^{-2} s^{-1}), R_n is the surface net radiation (W m^{-2}), G is the surface ground heat flux (W m^{-2}), Δ is the slope of the saturation vapor pressure curve at the temperature of interest (Pa K^{-1}), γ is the psychrometric constant (Pa K^{-1}), λ is the latent heat of vaporization (J kg^{-1}), ρ_a is the air density (kg m^{-3}), C_p is the specific heat of air (J kg^{-1} K^{-1}), D is the vapor pressure deficit (VPD, Pa), and Ga is the aerodynamic conductance (m s^{-1}). The variants of the Penman equation have been widely used to estimate PET in hydrological and land surface modeling (Sellers et al., 1996; Liang et al., 1994; Ek et al., 2003; Peng, Li, & Sheffield, 2018; Peng et al., 2019; Yang et al., 2019).

The open-water Penman (OW) equation is a simplified Penman equation to calculate PET over an open water surface, re-parameterized by Shuttleworth (1993):

$$PET_{OW} = \frac{\Delta}{(\Delta + \gamma)} \frac{(R_n - G)}{\lambda} + \frac{\gamma}{\Delta + \gamma} \frac{6.43(1 + 0.536 u_2) D}{\lambda} \qquad (2)$$

where PET_{OW} is typically in mm d^{-1} (kg m^{-2} s^{-1} = 86400 mm d^{-1}), $(R_n - G)$ is daily available energy (J m^{-2} d^{-1}), u_2 is the wind speed at 2-m height (m s^{-1}), λ is J kg^{-1}, and D is in kPa. Note that the OW equation provides daily estimates, and therefore some of the variables have different units compared to those in Equation 1.

Deleted: from

The Priestley-Taylor (PT) equation is also a simplified form of the Penman equation, which describes evaporation from a well-watered surface based on the equilibrium evaporation under conditions of minimal advection (Priestley & Taylor, 1972):

$$PET_{PT} = 1.26 \frac{\Delta(R_n - G)}{\lambda(\Delta + \gamma)} \qquad (3)$$

where PET_{PT} is in mm d^{-1} and $(R_n - G)$ is in J m^{-2} d^{-1}.

The Penman-Monteith (PM) equation (Monteith, 1965) is an extended version of the Penman equation to estimate actual ET (kg m^{-2} s^{-1}), which introduces the surface conductance (Gs, m s^{-1}):

$$PET_{PM} = \frac{\Delta(R_n - G) + \rho_a C_p D Ga}{\lambda\left(\Delta + \gamma\left(1 + \frac{Ga}{Gs}\right)\right)} \quad (4)$$

The reference crop evapotranspiration (PET_{RC}) recommended by the UN Food and Agricultural Organization (FAO) is a specific application of the Penman-Monteith equation (Allen, Pereira, Raes, & Smith, 1998). It is designed for calculating the maximum ET of reference crop under well-watered condition. The general formula is given by Allen et al. (2005):

$$PET_{RC} = \frac{0.408\Delta(R_n - G) + \frac{C_n u_2}{T_a + 273}\gamma D}{\Delta + \gamma(1 + C_d u_2)} \quad (5)$$

where PET_{RC} is also in mm d^{-1}, $(R_n - G)$ is daily available energy (MJ m^{-2} d^{-1}), Δ and γ are in kPa ^{o}C $^{-1}$, T_a is the air temperature at 2-m height (^{o}C), D is in kPa, C_n (K mm s^3 Mg^{-1} d^{-1}) is a constant describing the effect of aerodynamic conductance (Ga) that increases with canopy height. The denominator $\Delta + \gamma(1 + C_d u_2)$ is a special form of the denominator of the Penman-Monteith equation $\Delta + \gamma(1 + Rs/Ra)$. C_d ($\frac{Rs}{Ra\, u_2}$, s m^{-1}) is a constant that increases with the ratio of surface resistance ($Rs = 1/Gs$) to aerodynamic resistance ($Ra = 1/Ga$). There are two sets of C_n and C_d, tall crop (C_n=1600, C_d=0.38) and short crop (C_n=900, C_d=0.34). The FAO short crop equation is used in the recent version of the SPEI calculation (Beguería, Vicente-Serrano, Reig, & Latorre, 2013).

The above-mentioned equations treat the surface vegetation as a "big leaf" by considering the canopy resistance and soil resistance together as the bulk surface resistance, and therefore require fewer parameters and less computational costs. One challenge of the big-leaf assumption is to infer bulk surface resistance from canopy resistance when the surface is not fully covered by vegetation (Leuning et al., 2008). Additionally, we compare the big leaf models with the Shuttle-Wallace (SW) two source model (Shuttleworth and Wallace, 1985; Sun et al., 2023), incorporating vegetation cover and separating ET into the sum of transpiration and soil evaporation:

$$PET_{SW} = C_c PET_{PMc} + C_s PET_{PMs} \quad (6)$$

where the formulas and parameterizations of PET_{PMc}, PET_{PMs}, C_c, and C_s are given in the Appendix A.

3.2 Surface characteristics

Classical PET definitions rely on surface meteorology and do not faithfully represent the vegetation conditions and biophysical constraints and become less accurate over non-uniform land surfaces (Moran et

Deleted: 3

Deleted: 4

Deleted: The Priestley-Taylor (PT) equation is also a simplified form of the Penman equation, which describes evaporation from a well-watered surface based on the equilibrium evaporation under conditions of minimal advection (Priestley & Taylor, 1972): ... [1]

Moved up [2]: The above methods require observations or estimates of surface net radiation, near-surface temperature, wind speed, or specific humidity. Empirically based methods can induce large uncertainty in the drought projection (Sheffield et al., 2012; Feng, Trnka, Hayes, & Zhang, 2017) and are therefore not considered in the study.

Deleted: ; Zhou et al., 2006

Deleted: 13

Deleted: by Equations 12-18 in Shuttleworth and Wallace (1985). We adopt the same parameterizations detailed in Zhou et al. (2006).

al., 1996). To understand the impact of surface characteristics on the AED estimate and drought quantification, four factors are explored: (i) aerodynamic conductance, (ii) surface conductance, (iii) canopy height, and (iv) surface albedo. This section introduces the major options of formulas for these factors.

3.2.1 Aerodynamic conductance

Aerodynamic conductance Ga in the OW and PT methods (Equations 2 and 5) are implicitly derived from a smooth surface with low roughness length, which can underestimate the Ga and PET values in the forests (Peng et al., 2019). Open water aerodynamic conductance Ga_{OW} can be obtained by inverting the open water Penman equation (Equation 2) to match the Penman equation (Equation 1), given by Peng et al. (2019):

$$Ga_{OW} = \frac{6.43(1 + 0.536u_2) \cdot P_s}{86.4\epsilon\lambda\rho_a} \qquad (6)$$

where u_2 is converted from wind speed at 10-m to 2-m height following the wind profile relationship in Allen, Pereira, Raes, & Smith (1998). P_s is near-surface atmospheric pressure (Pa), ϵ is the ratio of molecular weight of water to dry air (= 0.622).

Short and tall reference crop aerodynamic conductance $Ga_{RC-short}$ and $Ga_{RC-tall}$ are given by

$$Ga_{RC-short} = \frac{u_2}{208} \qquad (7)$$

$$Ga_{RC-tall} = \frac{u_2}{110} \qquad (8)$$

where u_2 is converted from wind speed at 10-m to 2-m height (m s^{-1}).

Instead of the low Ga in OW and the fixed Ga in RC, it is better to generate more realistic surface roughness varying by land cover type, hereafter called Ga_{LC} (Brutsaert & Stricker, 1979; Allen, Pereira, Raes, & Smith, 1998; Shuttleworth, 1993):

$$Ga_{LC} = \frac{k^2 u_z}{\ln\left(\frac{z_m - d_0}{z_{0m}}\right)\ln\left(\frac{z_h - d_0}{z_{0h}}\right)} \qquad (9)$$

where z_m is the measurement height (m) for wind speed, z_h is the measurement height (m) for temperature and humidity, u_z is the wind speed at measurement height (m s^{-1}), k is the von Karman constant, d_0 is the zero-plane displacement height (m), z_{0m} and z_{0h} are the roughness lengths for momentum and heat (m). d_0 and z_{0m} can be estimated from canopy height (h) following d_0 = 2h/3 and z_{0m} = h/8 (Brutsaert, 1982). When estimating z_{0h}, instead of assuming $z_{0h} = 0.1z_{0m}$ as in Allen, Pereira, Raes, & Smith (1998), it is common

Deleted: three

Deleted: ii

Deleted: equations and

Deleted: 2

Deleted: is

Deleted: to use canopy height

to introduce a concept of excess resistance (Verma, 1989) and characterize the relationship between z_{0h} and z_{0m}:

$$z_{0h} = \frac{z_{0m}}{\exp(kB^{-1})} \tag{10}$$

The $\ln(z_{0m}/z_{0h})$ term, also known as kB^{-1}, depends on the roughness Reynold's number $Re*$ or frictional velocity ($u*$), LAI (Yang & Friedl, 2003), and land cover type (Rigden, Li, & Salvucci, 2018).

For the SW method, the two aerodynamic resistances are given by Eq. A11-17 (Appendix A).

3.2.2 Surface conductance

Deleted: 2

In previous PET methods, surface conductance is either not considered or assumed to be constant across vegetation types and over time. LAI plays a dominant role in determining the canopy-atmosphere coupling and ET partitioning (Peng et al, 2019; Wei et al., 2017; Forzieri et al., 2020). The OW and PT approach does not consider the role of LAI. The FAO approach uses a constant LAI throughout the growing season. Here we adopt a widely used method in estimating actual ET and assume a well-watered condition. The maximum surface conductance Gs_{max} can be obtained by scaling the maximum stomatal conductance (Gst_{max}) with LAI (Yan et al., 2012):

Deleted: the

Deleted: satellite data

$$Gs_{max} = Gst_{max} \cdot LAI \tag{11}$$

An alternative formula for Gs_{max} is from Zhou et al. (2006):

Moved down [3]: Kelliher, Leuning, Raupach, & Schulze (1995) found that Gs_{max} estimates are at most three times of the Gst_{max} estimates, therefore we set a maximum limit for LAI = 4. For Gst_{max}, the measured values are ranging from 9 mm/s for natural vegetation to 12 mm/s for crops (Kelliher, Leuning, Raupach, & Schulze, 1995), listed in Table 1.

$$Gs_{max} = \frac{LAI_e}{Rst_{min}} \tag{12}$$

where LAI_e is the effective LAI, which is equal to LAI/2 when LAI is greater than 4. Rst_{min} We introduce two options to incorporate an average LAI or the seasonal cycle of LAI into the surface conductance.

Deleted: The FAO approach only uses a fixed LAI throughout the growing season. However, LAI plays a dominant role in determining the canopy-atmosphere coupling and ET partitioning (Peng et al, 2019; Wei et al., 2017; Forzieri et al., 2020). In this study, we overcome this limiting assumption by introducing the seasonal cycle of LAI. Kelliher, Leuning, Raupach, & Schulze (1995) found that Gs_{max} estimates are at most three times of the Gst_{max} estimates, therefore we set a maximum limit for LAI = 4. For Gst_{max}, the measured values are ranging from 9 mm/s for natural vegetation to 12 mm/s for crops (Kelliher, Leuning, Raupach, & Schulze, 1995), listed in Table 1. ¶
We also used a

Moved down [4]: Rst_{min} is the minimum stomatal resistance, obtained by the land cover types listed in Table 1 from Zhou et al. (2006).

3.2.3 Canopy height

Canopy height (h) is a key parameter in determining aerodynamic conductance. The OW and FAO methods generally assume it to be constant across vegetation types and temporal scales. To address this limitation, we introduce two methods for estimating canopy height. The first method, eventually used to obtain d_0 and z_{0m} for Eq.9, determines canopy height based on land cover type by calculating the median height within each land cover from the global tree height dataset. The second method, applied in the SW two source model (Appendix A, Eq. A9-10), takes into account both land cover type and dynamic LAI. Each land cover type has a range for canopy height defined by the minimum canopy height (h_{min}) and maximum canopy height

(h_{max}). The actual canopy height is then determined by assuming a linear relationship with LAI following Zhou et al. (2006).

$$h = h_{min} + \frac{(h_{max} - h_{min})LAI}{LAI_{max}} \quad (13)$$

where LAI_{max} represents the annual maximum value at the grid cell level, obtained from the satellite data. Note that h is set to zero if LAI_{max} is zero.

3.2.4 Albedo

Deleted: 3

Current PET methods generally apply a uniform grass albedo value of 0.23 regardless of the underlying land cover type (Allen, Pereira, Raes, & Smith, 1998). To improve upon this assumption, we also introduce an option of introducing seasonal albedo cycle from satellite observations to both align albedo with specific land cover type and reflect temporal variations accurately.

Deleted: a fixed

Deleted: In this study

Deleted: the albedo consistent with the land cover type and explore the option

3.3 Parameterizations of surface characteristics

We use a simple look-up table approach to provide parameters based on land cover type (Fig. 1), summarized in Table 1.

Moved down [6]: Given that NLDAS-2 provides wind speed at a 10 m level, we used a measurement height = 10 m for both wind speed and temperature because the variation in the vertical temperature profile (2-10 m) is negligible compared to that of wind speed.

Deleted: roughness

Deleted: ,

Deleted: z_{0m}, d_0, kB^{-1},

Moved (insertion) [6]

Deleted: G

Moved down [5]: z_{0h} is then estimated based on land cover specific z_{0m} and kB^{-1} (Equation 10).

For Eq. 9, given that NLDAS-2 provides wind speed at a 10 m level, we used a measurement height = 10 m for both wind speed and temperature because the variation in the vertical temperature profile (2-10 m) is negligible compared to that of wind speed. z_{0h} is then estimated based on land cover specific z_{0m} and kB^{-1} (Equation 10). For z_{0m}, we apply the typical values based on median canopy height for different land cover types, and estimated d_0 from z_{0m} ($d_0 \approx 16z_{0m}/3$).

For kB^{-1}, we adopt estimates from a collection of literature as below. The forests generally have lower kB^{-1} values (kB^{-1} = 1 for needleleaf or mixed forest, kB^{-1} = 0.5 for broadleaf) than shrublands (kB^{-1} = 3.75) and croplands (kB^{-1} = 1.75), based on the values of Rigden et al. (2018) for the medium emissivity case (ϵ = 0.96). For grasslands, kB^{-1} = 2.25 is computed as the average of short grass (kB^{-1} = 2.0) and medium-length grass (kB^{-1} = 2.5), based on Brutsaert (1982). For barren or bare soil, we estimate kB^{-1} = 3 by taking the average of all observed kB^{-1} in Yang et al. (2008). Nadeau et al. (2009) suggested kB^{-1} = 6 for the urban area. For water body, wetlands, and snow, we adopt the widely-used kB^{-1} = 2, as Zilitinkevich et al. (2001) showed that kB^{-1} over the water surface is within the 0~4 range. There are large variations in the observed kB^{-1} for savannas. Troufleau et al. (1997) reported kB^{-1} = 7.9 for fallow savanna; Kustas et al. (1989) provided a range of 1 to 11; Stewart et al. (1994) found an average value of kB^{-1} = 5.8, similar to the study by Lhomme et al. (1997) that reported kB^{-1} = 5.9 for Sahelian vegetation; Verhoef et al. (1997)

suggested a high value of $kB^{-1} = 12.4$. We choose $kB^{-1} = 7$ as most of these observed values fall into the range of 6-8.

z_{0h} is then estimated based on land cover specific z_{0m} and kB^{-1} (Eq. 10).

To calculate surface conductance in Eq. 11-12, we provide two set of parameterizations based on land cover type. The first set is derived from the findings of Kelliher, Leuning, Raupach, & Schulze (1995). For Gst_{max}, the measured values are ranging from 9 mm/s for natural vegetation to 12 mm/s for crops, as detailed in Table 1. They also found that Gs_{max} estimates are at most three times of the Gst_{max} estimates, therefore we set a maximum limit for $LAI = 4$. The second set uses the minimum stomatal resistance Rst_{min}, following Zhou et al. (2006), also listed in Table 1.

Table 1. Ga and Gs parameters by IGBP land cover*.

ID	Code	Name	z_{0m} (m)	d_0 (m)	kB^{-1}	Gst_{max} [j] (mm s^{-1})	Rst_{min} [k] (s m^{-1})
0	WB	Water body	0.0004 [a]	0.002	2.0 [e]	NA	NA
1	ENF	Evergreen needleleaf	1.1 [b]	5.9	1.0 [f]	9.3	150
2	EBF	Evergreen broadleaf	1.1 [b]	5.9	0.5 [f]	9.3	150
3	DNF	Deciduous needleleaf	0.9 [b]	4.8	1.0 [f]	9.3	150
4	DBF	Deciduous broadleaf	0.9 [b]	4.8	0.5 [f]	9.3	150
5	MF	Mixed forest	0.9 [b]	4.8	1.0 [f]	9.3	150
6	CSH	Closed shrublands	0.2 [a]	1.1	3.75 [f]	9.3	150
7	OSH	Open shrublands	0.2 [a]	1.1	3.75 [f]	9.3	100
8	WSA	Woody savannas	0.4 [a]	2.1	7.0 [g]	9.3	180
9	SAV	Savannas	0.4 [a]	2.1	7.0 [g]	9.3	120
10	GRA	Grasslands	0.05 [a]	0.27	2.25 [a]	12	115
11	WET	Permanent wetlands	0.04 [c]	0.21	2.0 [e]	12	65
12	CRO	Croplands	0.12 [d]	0.64	1.75 [f]	12.2	90
13	URB	Urban and built up	1.1 [b]	5.9	6.0 [h]	NA	NA
14	MOS	Cropland/vegetation	0.12 [d]	0.64	1.75 [f]	12.2	120
15	SNO	Snow/ice	0.00001 [a]	5.3E-05	2.0 [e]	NA	NA
16	BSV	Barren	0.01 [d]	0.053	3.0 [i]	NA	NA

*The above estimates are collected from [a]Brutsaert (1982), [b]Campbell and Norman (1998), [c]Acreman et al. (2003), [d]Monteith and Unsworth (2013), [e]Zilitinkevich et al. (2001), [f]Rigden et al. (2018), [g]Kustas et al. (1989), Stewart et al. (1994), Troufleau et al. (1997), Lhomme et al. (1997), and Verhoef et al. (1997), [h]Nadeau et al. (2009), [i]Yang et al. (2008), [j]Kelliher et al. (1995), [k]Zhou et al. (2006).

4 Evaluation of the PET methods and parameterizations

4.1 Drought quantification: SPEI vs. soil moisture

Moved (insertion) [5]

Moved (insertion) [3]

Deleted: ,

Deleted: t

Deleted: For Gst_{max}, the measured values are ranging from 9 mm/s for natural vegetation to 12 mm/s for crops (Kelliher, Leuning, Raupach, & Schulze, 1995), listed in Table 1.

Moved (insertion) [4]

Deleted: Rst_{min} is the minimum stomatal resistance

Deleted: obtained by the land cover types

Deleted: listed in Table 1 from Zhou et al. (2006)

Given the substantial divergence in the PET magnitudes among different models (Peng et al., 2019), a direct comparison of the absolute values among methods is not meaningful. However, the performance in representing drought between PET methods should be comparable. We hypothesize that incorporating the parameters or model structures in Section 3 into the existing methods will increase the accuracy of drought quantification.

Deleted: To test the hypotheses, we use the PM algorithm for big leaf methods, so that we can easily control a specific set of parameters that represents a process option.

We integrate the PET methods into the SPEI drought index across 1-, 3-, 6-, and 12-month time scales over the CONUS for the period of 1981-2017. The SPEI is based on the climatological water balance (water supply – atmospheric evaporative demand) cumulated over multiple time scales (e.g., 1, 3, 6, 12 months) following a similar procedure as in the SPI computation (Vicente-Serrano, Beguería, & López-Moreno, 2010). The accumulated water balances are fit using the log-logistic distribution and the probability distribution function is normalized to a standardized variable with mean = 0 and standard deviation = 1, termed as 1-, 3-, 6-, 12-month SPEI, respectively. We calculate the monthly SPEI with the SPEI R package (https://cran.r-project.org/web/packages/SPEI/) using daily meteorological data. We choose the SPEI driven by zero PET as a control scenario to showcase the net effect of introducing existing PET methods into traditional SPI drought index. We choose the SPEI driven by the Open Water (OW) method as the reference method, because the OW approach is the simplest scenario with minimal surface characteristics.

Deleted: baseline

Soil moisture is a direct measure of drought severity. Therefore, we use the correlation between SPEI and soil moisture observations to quantify the skill of PET methods. We aggregated the daily ESA CCI surface soil moisture (SMsurf, m^3 m^{-3}) to monthly averages between 1981-2017 over the CONUS. To match the SPEI on multiple time scales, we calculated the moving average of SMsurf for 1, 3, 6, 12-month periods, respectively. Our analysis focuses on the growing season (April-September), because PET is close to zero during the cold season (not shown). Given the monthly SPEI and SMsurf series during the growing season, Pearson correlation coefficient (R) is calculated for each pair of the SPEI and SMsurf monthly series in each grid cell of the CONUS on the time scale of 1, 3, 6, and 12 months. Then we calculate the change of correlation for each method from the control scenario or the reference. This change can identify whether a PET method causes an improvement in drought quantification relative to the reference approach.

Deleted: baseline

Deleted: baseline

4.2 Initial examination of surface characteristics

Deleted: 3.3 Two source model: separating canopy and soil¶

We conducted a pilot analysis to identify the relative importance of different surface characteristics. To test the hypotheses, we use the PM algorithm for big leaf methods, so that we can easily control a specific set of parameters that represents a process option. Each of the above processes are regarded as different options: (i) using active surface roughness or open water surface, (ii) seasonally varying or fixed surface conductance, and (iii) seasonally varying or fixed surface albedo. Table 2 provides the PET methods and the parameters in the preliminary analysis. We selected four existing PET methods and seven testing methods. The first set of methods (a-d) are the existing physically-based PET approaches: the open-water Penman equation (OW), the FAO reference crop evapotranspiration for tall crop and short crop, and the Priestley-Taylor equation (PT).

First, in methods (e), (f), (g), the aerodynamic conductance module is not active as we set Ga to the open water Ga_{ow}, indicating a smooth surface with low roughness (Eq. 6). In methods (h), (i), (j), (k), we activate the aerodynamic conductance using realistic surface roughness (Eq. 9). Second, in methods (e), (i), (j), the surface conductance parameter is unconstrained as we set Gst_{max} to infinity. In methods (f), (g), (h), (k), we activate the surface conductance using seasonal LAI dynamics and Gst_{max} from Kelliher et al. (1995). Lastly, in methods (f), (i), (k), the albedo parameter is not active as we set α to a constant (grass: 0.23, water: 0.08). In methods (e), (g), (h), (j), we activate the albedo parameter using seasonal albedo dynamics.

Table 2. Summary of the PET methods with their ID, name and abbreviation code, and details about surface characteristics.

		Ga		Gs_{max}			Albedo (α)	
ID	Method (Code)	Open Water	Rough surface	Infinite	Constant	Seasonal	Constant	Seasonal
a	Open Water (OW)	X		X			X	
b	FAO Tall reference crop (RC-tall)		X		X		X	
c	FAO Short reference crop (RC-short)		X		X		X	
d	Priestley-Taylor (PT)						X	
e	Open Water Ga/ Infinite Gs/ Seasonal α (GAow_GSinf_ALBs)	X		X				X
f	Open Water Ga/ Seasonal Gs/ Constant α (GAow_GSs_ALBc)	X				X	X	
g	Open Water Ga/ Seasonal Gs/ Seasonal α (GAow_GSs_ALBs)	X				X		X
h	Rough Ga/ Seasonal Gs/ Seasonal α (GAr_GSs_ALBs)		X			X		X
i	Rough Ga/ Infinite Gs/ Constant α (GAr_GSinf_ALBc)		X	X			X	
j	Rough Ga/ Infinite Gs/ Seasonal α (GAr_GSinf_ALBs)		X	X				X
k	Rough Ga/ Seasonal Gs/ Constant α (GAr_GSs_ALBc)		X			X	X	

*Note that many methods in these experiments are unrealistic due to the inconsistencies of the surface conditions. Our attention is to include as many combinations as possible for a preliminary analysis.

In Section 5.1, we compare the CONUS averaged R values between the pairs of PET methods that share the same surface characteristics except for one of the features (see Fig. 3). The first feature surface roughness is determined by the way Ga is estimated. We compare the parameter set between rough and the open water surface by calculating the differences (Rough - Open Water) for the following pairs of experiments including (i) GAr_GSinf_ALBc - (a) OW, (j) GAr_GSinf_ALBs - (e) GAow_GSinf_ALBs, and (k) GAr_GSs_ALBc - (f) GAow_GSs_ALBc. In terms of the canopy conductance, we calculate the differences between seasonal and infinite Gs_{max} (Seasonal - Infinite) for the following pairs of experiments: (f) GAow_GSs_ALBc - (a) OW, (g) GAow_GSs_ALBs - (e) GAow_GSinf_ALBs, and (k) GAr_GSs_ALBc - (i) GAr_GSinf_ALBc.

4.3 Comparison of PET parameterizations

Based on the results of section 5.1, we further examine different parameterizations for Ga and Gs in order to identify optimal PET algorithms (shown in Section 5.2). We establish a control scenario where PET is not considered at all in the SPEI, equivalent to the traditional SPI. The PET methods under consideration have two categories, the big leaf model and the two source model (Fig. 4 left table). The big leaf model include three traditional methods (Open Water [OW], Reference Crop for short [RC-short], and tall [RC-tall] crops) and two land cover dependent (LC) methods. The LC method uses the same aerodynamic conductance method (Eq. 9) but differ in their surface conductance parameterizations: LC-Kelliher, which adopts Gst_{max} from Kelliher, Leuning, Raupach, & Schulze (1995), and LC-Zhou, which uses Rst_{min} from Zhou (2006). Additionally, for each big leaf model, alternative Gs parameterizations based on either OW or RC-short are provided for comparative purpose, even though they are not considered unrealistic. We then calculated ΔR between each PET method and the control scenario (set PET to zero).

5 Results

5.1 Initial assessment of surface characteristics

We conducted a preliminary analysis to identify the relative importance of different surface characteristics. We examine seven algorithms (e-k) to isolate the effects of surface characteristics on PET (Table 2). Fig. 2 displays the spatial patterns of growing season averages of these methods. For the classical Penman/Penman-Monteith methods (Fig. 2a-c), the highest mean growing season AED values are found in southern California, Arizona, and Texas, while the PT method (Fig. 2d) predicts the largest AED values in Texas and Florida. The spatial patterns of PET based on the rough surface (Fig. 2h-l, Rough Ga) are very different from those methods that assume a universal reference height (Fig. 2b-c, reference crop) or open water surface (Fig. 2a, e-g). Specifically, the regions which exhibit large PET estimates (> 250 mm/mon, Fig. 2h-k) are forests, such as ENF in the Pacific Northwest, DBF in the Northeast, and MF in the southeastern U.S.. Interestingly, although the methods using constant albedo (α=0.08) have generally larger AED values than those using seasonal albedo, the differences in the spatial pattern between the two are almost negligible (Fig. 2a vs. e, i vs. j, k vs. h). The combination of the rough aerodynamic and unconstrained surface conductance, represented by (i) and (j), produces extremely high monthly PET values with means at 330 to 340 mm/mon. The remaining methods also predict a wide range of mean monthly totals. On average, the big-leaf method (Fig. 2h) provides the most constrained (smallest) PET estimates.

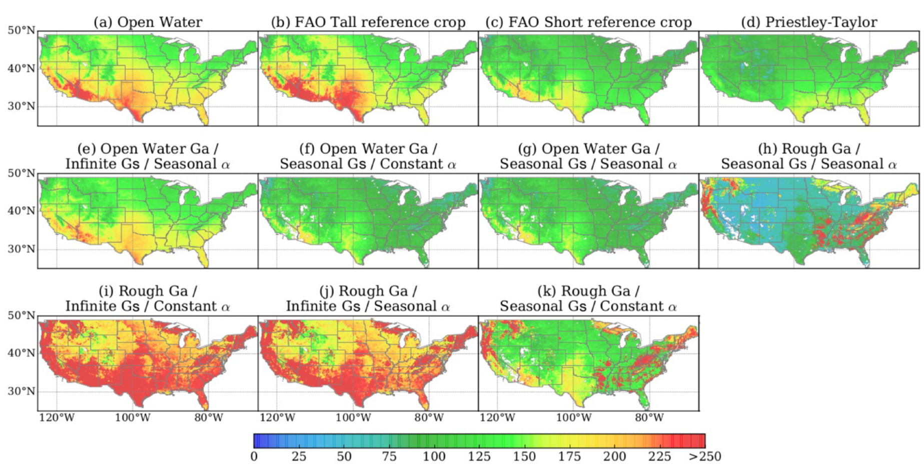

Figure 2. Growing season averages of AED derived from four PET methods and seven testing algorithms over the CONUS. Details and ID for each method are listed in Table 2.

Deleted: Overall

Deleted: evaluation

Deleted: the PET parameterizations

Deleted: pilot

Assessing the change between pairs of the above methods can identify whether adding/removing a surface feature eventually causes an improvement in drought quantification (Fig. 3). Interestingly, activating realistic surface roughness does not necessarily increase, but may even decrease the correlation (ΔR ranging from -0.01 to 0.01 for all time scales). Canopy conductance stands out to be the most important feature for enhancing the skill of drought index (ΔR = 0.015-0.03), meaning that adding the plant phenology driven by LAI can largely improve the seasonal variations of drought index and hence the correlation with SMsurf. We compare ΔR of four pairs with an inconsistent surface (e.g., a combination of open water Ga and seasonal Gc) subtracting from a consistent surface and find that methods with consistent surface features have higher correlations with SMsurf. Surprisingly, seasonal and constant albedo showed no significant difference on the correlations, possibly because of the little variation of albedo during the growing season. The differences in the spatial pattern between constant and seasonal albedo are almost negligible (Fig. 2). In subsequent sections, we default to using the seasonal albedo in our PET methods to fully represent the surface characteristics.

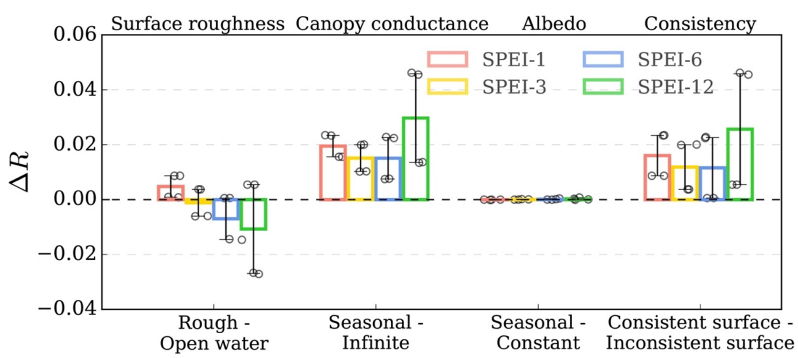

Figure 3. Differences in spatially averaged correlation (ΔR) of pairs of PET methods that share the same surface characteristics except for one of the surface features: surface roughness, canopy conductance, albedo, and overall consistency among the above features. The white dots indicate the average ΔR between the four methods and the reference method.

Deleted: We selected four existing PET methods and seven testing methods (see Table A1 and Fig. A1 in Appendix A). Note that many methods in these experiments (Table A1) are unrealistic due to the inconsistencies of the surface conditions. Our attention is to include as many combinations as possible for a preliminary analysis. We then compare the CONUS averaged R values between the pairs of PET methods that share the same surface characteristics except for one of the features (Fig. 2).

5.2 Performance of PET parameterizations

Fig. 4 shows ΔR between each PET method and the control scenario (set PET to zero) for all grids, forested grids, and nonforested grids using 1-month SPEI. The big leaf methods are grouped by the parameterization of Ga and Gs. Incorporating the benchmark OW method into the SPEI increases R by 0.042, shown by the top horizontal bars. Among the conventional PET methods, the tall reference crop (RC-tall) method stands out. Over the CONUS, it improved ΔR relative to control scenario by 29% more than the OW method (0.054 versus 0.042). The short reference crop (RC-short) method has an identical averaged R with the OW method. Although the RC-tall algorithm (Allen et al., 2005) is less known than the widely used RC-short algorithm (Allen, Pereira, Raes, & Smith, 1998), our results suggest that the SPEI driven by RC-tall correlates better with the SMsurf dynamics.

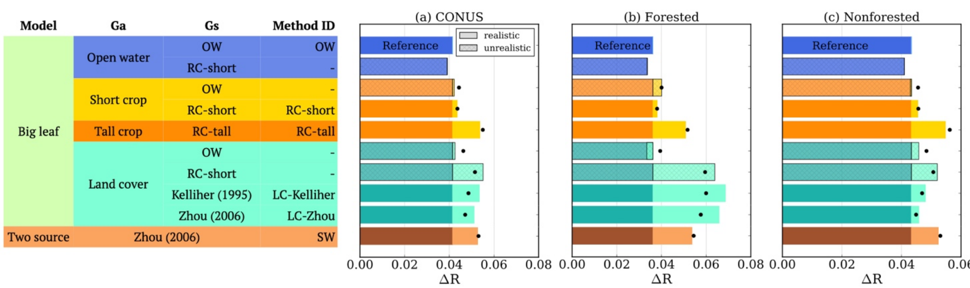

Figure 4. Differences in correlations (ΔR) for selected PET methods versus the control scenario (PET = 0). Correlations were computed between the 1-month SPEI and SMsurf series across: (a) CONUS, (b) forested grids, and (c) nonforested grids. The bars represent the mean ΔR and the black dots represent the median ΔR. The top blue bars show ΔR in the OW approach versus PET = 0 as a reference. For each bar, the darker shade indicates the reference ΔR and the lighter shade represents any improvement (or decline) relative to the reference. Methods with unrealistic surface conditions are highlighted with a hatch pattern, without any specific Method ID.

One encouraging outcome is the performance improvement seen in the two big leaf algorithms incorporating realistic surface conductance. Activating both surface roughness and seasonal Gs produces high correlations of SPEI with SMsurf. These algorithms improve the OW method (ΔR = 0.042) by 24-29% (ΔR is 0.052-0.054). Methods where Ga is determined by land cover (the cyan bars in Fig. 3a) especially improve the correlations with SMsurf (Fig. 3a). It confirms our hypothesis that incorporating realistic vegetation information in atmospheric evaporative demand can enhance drought characterization. Finally, the two

Deleted: We further compare different parameterizations for Ga and Gs. Here we establish a control scenario where PET is not considered in the SPEI, equivalent to the traditional SPI. The selected PET methods include three traditional methods: OW, RC-short, and RC-tall, four big leaf models and a two source model. We calculated ΔR between each PET method and the control scenario (set PET to zero).

Deleted: 3

source Shuttleworth-Wallace (SW) method outperforms the OW method as expected. However, the SW method produces a similar R as the LC-Kelliher method. This suggests that the simple big leaf model in combination with the land cover details can achieve the same efficacy of the more complicated two source model. While we evaluated several unrealistic methods (see hatch patterns) with inconsistent surface assumptions, most did not outperform the OW method. One exception is the pairing of land cover-specific Ga with the RC-short Ga, which yields a high R.

Over the CONUS, RC-tall, LC-Kelliher, and SW are the top three methods with similar average R. However, when we evaluate the performance in the forested areas (Fig. 3b), LC-Kelliher exhibits the most significant enhancement in ΔR to control scenario, with an increase of 89% over OW's improvement (0.068 relative to 0.036). RC-tall and SW improve ΔR to control scenario by 39% (0.05) and 50% (0.054), respectively. In nonforested areas (Fig. 3c), RC-tall has the best performance, followed by SW. The SW method, designed for sparse vegetation, naturally demonstrates strong performance in these regions. However, it is surprising to see that the simple parametrized RC-tall can outperform SW. Conversely, LC-Kelliher only exhibits a moderate improvement in ΔR. This suggests that, particularly in the sparsely vegetated areas, RC-tall can serve as a strong candidate for PET estimates and drought characterization.

5.3 Spatial patterns analysis

Deleted: 2

In the subsequent sections, we compare the LC-Kelliher (referred to as LC) method with the three widely used methods: OW, PT, RC-short (simply referred to as RC), and the two source SW method. The time series of these PET methods as well as the SMsurf time series are shown in the Fig. 5. The OW approach serves as the reference. The highest R is observed for long-term drought (12-month, average R = 0.73) and the lowest is found in medium-term drought (3- and 6-month, average R = 0.48). This suggests that the meteorology-driven SPEI can generally reproduce soil moisture dynamics, especially on an annual time scale.

Deleted: B1

Deleted: baseline

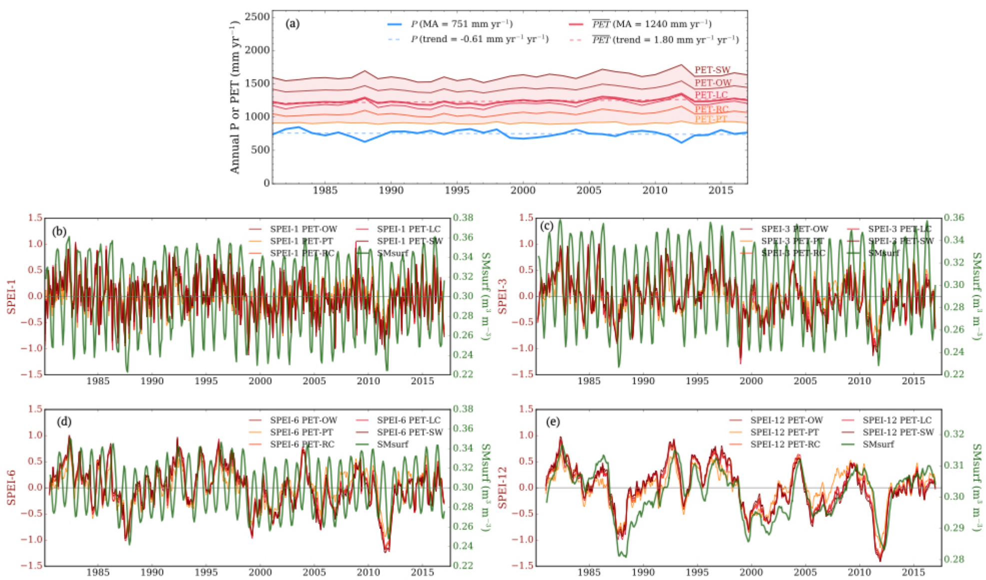

Figure 5. Temporal evolution of PET methods, SPEIs, and SMsurf. a) The annual precipitation and PET (mm yr^{-1}) from five key methods between 1981-2017. b)-e) SPEI series driven by the five PET methods, aligning with the SMsurf time series for four time scales: 1, 3, 6, 12-month.

Deleted: T

Fig. 6 displays the spatial distribution of correlations between SPEI driven by OW and SMsurf, along with the differences in correlations of PT, RC-short, LC, and SW compared to OW. PT consistently exhibits lower correlations than OW over most regions, with an average decrease of 0.04, and has especially weak correlations in the southwest U.S. (lower by 0.15). Interestingly, the widely used RC method for SPEI

Deleted: ure

Deleted: 4

presents little improvement over OW with minimal increases in correlation. LC shows substantial improvements in some areas , with ΔR exceeding 0.16, notably in the eastern and pacific western U.S.. The enhancements of LC are prominent but can be diluted when averaged across CONUS, with ΔR relative to the control scenario 0.012 higher than OW (Fig. 4a). This is especially true when considering LC's less favorable performance in the wouthwest and midwest U.S.. SW also exhibits notable improvements in the eastern and pacific western U.S., with a magnitude of improvement falling between LC and RC. It is encouraging to see that LC outperforms SW in many eastern US grid cells (ΔR = 0.15 versus ΔR = 0.05), given LC's much simpler parameterization. Though it is worth noting that both LC and SW experience performance declines in the Southwest, with LC slightly worse than SW. On the other hand, RC robustly displays improvements in this particular area.

Deleted: 3a

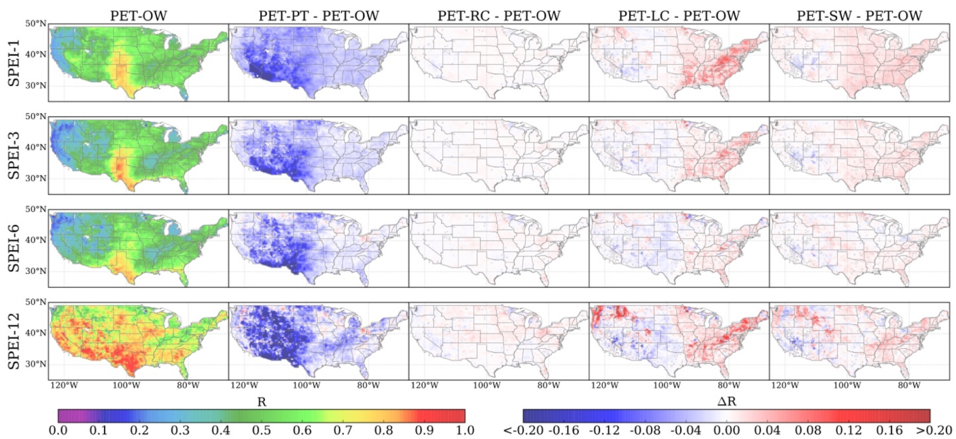

Figure 6. The first column displays the correlations between SPEI driven by OW and SMsurf. The four columns on the right show the differences in correlations (ΔR) of PT, RC, LC, and SW relative to OW.

We further delve into the relative performance of these methods summarized by major vegetation types and by aridity (Fig. 7). LC increases R significantly in forests, especially in evergreen broadleaf, deciduous broadleaf, and mixed forests, where the largest ΔR exceeds 0.1, and the average ΔR hovers around or above 0.05 for 1-month scale (Fig. 7a). Notable improvements in evergreen needleleaf forest, woody savanna, and croplands compared to the OW are also observed.

Deleted: 5

Deleted: 5a

For the time scale of 12-month (Fig. 7c), OW has an already high the average R of 0.73 across the CONUS. LC's performance is outstanding in forests, with an average ΔR of about 0.05 and the largest ΔR even exceeding 0.25. In evergreen needleleaf forests, LC's performance is significantly higher than that of the 1-month time scale. In humid regions, LC's improvements over SW becomes even more apparent compared to the 1-month time scale (Fig. 7d).

Deleted: 5c

Deleted: 5d

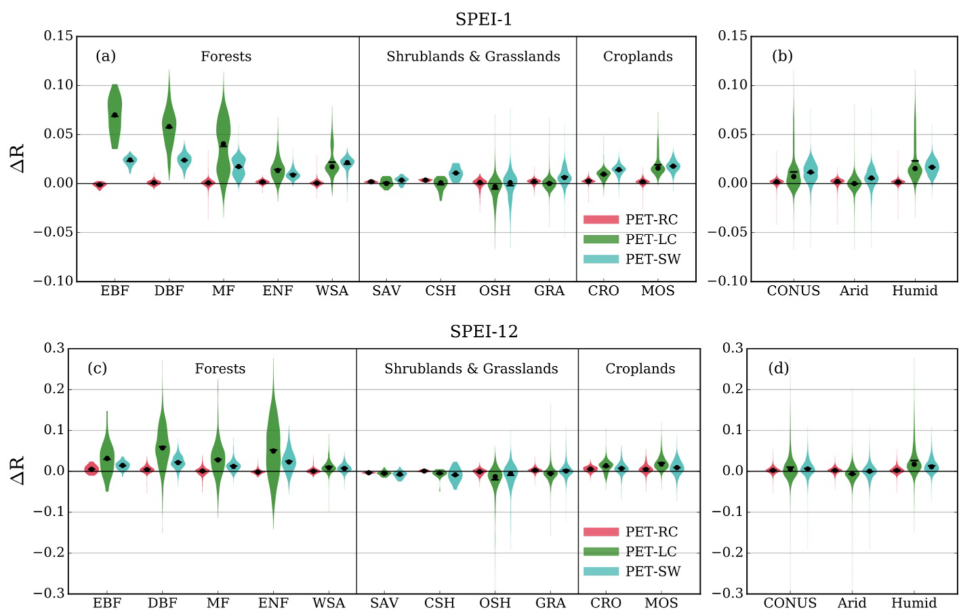

Figure 7. Violin plots of differences in correlations of three PET methods relative to OW, grouped by vegetation types and aridity.

In contrast, the average performance of LC in grasslands, shrublands, and savannas (Fig. 7a and c), which are the dominant vegetation types in the western CONUS, are equivalent to OW (except for open shrubland where LC slightly underperforms OW). The magnitude of averaged ΔR of LC is slightly smaller than SW, mainly due to LC's weaker performance in the arid shrublands and grasslands, which cover large portions of the CONUS. Both LC and SW show less advantage or even worse performance than RC and OW in nonforested and arid grid cells (Fig. 7c-d).

Deleted: 5a

Deleted: 5c

6 Discussion

6.1 Interaction between surface features

Fig. 3 provides important insights into the SPEI sensitivity to different surface features. Introducing Gs with seasonal vegetation dynamics accounts for most of the total improvement of PET algorithm. This confirms that the FAO approaches are more favored than the OW approach due to its constraints on Gs. This highlights the importance of leaf area index (LAI) as a vegetation feature for drought depiction. LAI is a scaling factor to upscale Gst_{max} to maximum canopy conductance. This is different from the drought index based on the normalized difference vegetation index (NDVI) or LAI, which requires the real-time dynamics of satellite data. This approach only requires the climatology of LAI, which can be easily implemented for drought forecasting where real-time or near-future data are not available.

Deleted: 2

Using realistic surface roughness does not necessarily improve the overall performance of the SPEI. In fact, the consistency between aerodynamic conductance and surface conductance is more critical for the skill of PET method. Previous study by Peng et al. (2019) explains the linkage between the ratio of actual ET to PET and the ratio of Ga to Gs. When Ga/Gs is large, the ratio of actual ET to PET becomes smaller. Although our study focused on the maximum evapotranspiration given the realistic vegetation condition, such a relationship remains valid. Thus, a large Ga/Gst_{max} ratio should better limit PET with realistic surface constraints. In fact, the LC approach activates surface roughness and increases Ga, while constraining Gst_{max} and reducing Gs. Altogether these factors increase the Ga/Gs ratio and result in significant improvement in capturing the temporal evolution of SMsurf.

6.2 Surface characteristics matter in the forests

Our analysis concludes that incorporating surface features can largely improve the accuracy of drought monitoring in the forests. There are two vegetation groups with significantly improved correlation after incorporating the realistic surface characteristics. Forests over the eastern and pacific western U.S., such as evergreen broadleaf and deciduous broadleaf forests, the LC method exhibits large ΔR compared to OW (up to 0.12 for 1-month and up to 0.25 for 12-month, Fig. 5a, c). While OW has a ΔR at about 0.04 compared to the zero PET control scenario (Fig. 3b), LC has an average ΔR of 0.05 relative to OW in these forests (Fig. 5a). This means the improvement of LC over control scenario is more than doubling of OW. LC also displays a significant increase in R at about 0.025 in woody savanna. The enhancements in the forests or woody savannas are the most predominant since LAI in forests is relatively variable, and surface roughness is also the strongest. Although the southeastern U.S. has a humid subtropic climate, this region also suffered from periodic droughts in 1986–1988, 1998–2002 and 2006–2009 (Seager, Tzanova, & Nakamura, 2009; Pederson et al., 2012), which is consistent with the increased forest drought severity from 1987-2013 (Peters, Iverson, & Matthews, 2014; Clark et al., 2016). Drought monitoring in these regions is also critical and can benefit from our approach that significantly improve the spatial and temporal accuracy in the forests. In addition, future improvements to our approach could benefit from incorporating newly available datasets such as Lang et al. (2023) for canopy height.

In contrast, the short-grass regions (grasslands, shrublands, and savannas) located in the western U.S. exhibit minimal improvements for LC. Given that the RC-tall method—a similar big leaf model—performs better than LC in these areas (Fig. 4), it suggests that uncertainties in LC's Gst_{max} could result in these outcomes. Additionally, a comparison between Gst_{max} and Rst_{min} (used in SW) highlights uncertainties in this parameter. For instance, Rst_{min} in shrublands, grasslands, and savannas ranges from 100-180 s m^{-1} (equivalent to Gst_{max} of 5-10 mm s^{-1}), which is generally lower than 9-12 mm s^{-1} reported by Kelliher et al. (1995). These findings highlight the need for in-situ measurements of surface conductance in these areas.

Deleted: zero to small

Deleted: These regions have sparse vegetation cover, and thus LAI plays a less effective role in determining the seasonal dynamics of PET.

Furthermore, these areas have sparse vegetation cover, and thus LAI plays a less effective role in determining the seasonal dynamics of PET. In the meantime, these areas are located in the arid regions (Fig. 7), the improvements of PET do not have significant effects on modeling the soil moisture, and precipitation dynamics may dominate the soil moisture variations.

6.3 Strategies for PET method selection

The LC method not only provides modest absolute PET values (Fig. 5a) but also displays better performance across many areas (Fig. 6). Specifically, LC estimates an annual PET of roughly 1200 mm, consistent with PET estimations for the same region as well as temperate zone reported in a recent study (Fig.8 in Sun et al., 2023).

We recommend the use of the LC parameterization for drought monitoring in the forests, in which the roughness and surface conductance parameters vary with realistic vegetation conditions. LC is superior than OW or RC-short because of better performance, and compared to SW, it is both better performing and a simpler approach in the forested areas.

For shrublands and grasslands, we recommend the use of RC-tall to replace the more widely used RC-short for drought monitoring. We found that the RC-tall approach has a higher skill than the RC-short approach that is more widely used. The main difference between these two methods is the C_n constant that describes the effect of aerodynamic conductance (Allen et al, 2005). The implementation of tall reference (C_n = 1600) seems to work better than the short reference (C_n = 900) over the CONUS. It is worth noting, however, that the FAO approaches assume a universal C_n regardless of actual vegetation type. The better skill of RC-tall will not always hold, which may overestimate PET in semi-arid non-vegetated regions.

For sparse vegetation, since the responses of the components of evapotranspiration to the environmental drivers are different (Katul, Oren, Manzoni, Higgins, & Parlange, 2012; Or & Lehmann, 2019), the partitioning between canopy and soil can also play a role in determining AED. The SW model significantly improves the SPEI skill driven by the OW approach. It outperforms LC in the shrublands and grasslands. Despite its complexity, it is a good choice for drought monitoring in these vegetation types (Sun et al., 2023).

For croplands, we recommend choosing between RC-tall versus RC-short based on the actual crop canopy height. The more realistic approach is to use RC-tall for higher crops. Lastly, the PT method has the poorest correlation with soil moisture and is unlikely to capture drought dynamics.

6.4 Bridging gaps in drought prediction

Motivated by the question of whether incorporating surface characteristics can improve drought prediction, we overcome several limitations of previous drought quantification methods. Firstly, our study presents a different approach whereby we focus on the maximum possible evapotranspiration for a given vegetation condition. This concept allows a physically meaningful definition of evaporative demand for the non-uniform land surfaces.

Secondly, the ultimate goal of PET calculation is to simulate ET and to quantify drought. Despite the simplicity of calculating PET using the existing Penman-type methods, the biggest challenge for assessing these methods is validation. Since the real evaporative demand rate is unattainable from observations, it is challenging to validate which PET method is superior directly. Even using ET observations for PET validation can be problematic because biased PET estimates and wrong surface biophysical parameters can still produce accurate ET estimates for locations with ET measurements (Peng et al., 2019). Our study evaluates the PET methods by comparing drought index with independently observed soil moisture (Vicente-Serrano et al., 2012). This approach helps diagnose the most appropriate PET approach for drought quantification directly while avoiding the complexity and divergence caused by various PET definitions. While the absolute improvements in correlation with soil moisture appear modest, they represent significant percentage changes of 25-30% and notable local improvements. We acknowledge the need for evaluation of the effectiveness in addition to the temporal correlations. Specifically, future studies should evaluate the capability of the land cover specific approaches to accurately capture extreme events.

Finally, our approach bridges the gap between the two methodologies for quantifying soil-moisture drought, which is of most relevance to agriculture (Seneviratne, 2012). Since soil moisture observations are limited by inadequate measurement networks, drought indices such as the SPEI are often used to quantify drought. In hydrology, a drought index is a simple water balance model driven by surface meteorology without the use of any surface characteristics. Its shortcomings are the neglect of seasonally varying vegetation cover and the incapability to capture the vegetation control on transpiration. An alternative is to use land surface models to estimate large-scale soil moisture (Sheffield, & Wood, 2007). This approach often builds in vegetation dynamics and can provide temporally consistent soil moisture simulations, but it also requires substantial efforts to prepare meteorological forcings at high temporal resolution, set up the domain, spin up, and calibrate. Our approach is a compromise between the above two types of models, which is more realistic and process-based than the commonly used drought index while being easy-to-implement and less data-intensive than a land surface model.

7 Conclusions

To understand whether incorporating surface characteristics can improve drought prediction, we revise current PET methods in a newly developed drought index (SPEI), using the concept of maximum ET for any given vegetation condition. We use a simple look-up table approach combining in situ measurements and large-scale data fusion products for the key surface and aerodynamic parameters,. This study also presents a novel application of independent soil moisture observations to diagnose the most appropriate PET approach for drought quantification. Our approach is proved to be more effective than widely used big leaf methods and two source model in accurately predicting soil moisture spatiotemporal dynamics in the forests and humid regions. LAI has a particularly important influence on the skill of the SPEI. This new yet simple approach strikes a balance between a meteorology-driven water balance model and a complex land surface model for drought prediction. It could improve the accuracy of the drought reconstruction in forests and displays great potential to improve real-time drought forecast.

Appendix A. Shuttleworth-Wallace Model

The Shuttleworth-Wallace (SW) two source model was developed to more accurately represent evapotranspiration from the sparse vegetation. Different from the big leaf models, SW treats the surface as a two-component structure: sparse vegetation (e.g., row crops) and soil. The following formulas are adapted from Equations 11-18 in Shuttleworth and Wallace (1985).

$$PET_{SW} = C_c PET_{PM}^c + C_s PET_{PM}^s \tag{A1}$$

where PET_{PM}^c and PET_{PM}^s are Penman-Monteith like combined equations (Eq. 4) for a closed canopy and bare soil. Each term is given by the following formulas

$$PET_{PM}^c = \frac{\Delta(R_n - G) + (\rho_a C_p D - \Delta r_a^c (R_n^s - G))/(r_a^a + r_a^c)}{\lambda\left(\Delta + \gamma\left(1 + \frac{r_s^c}{r_a^a + r_a^c}\right)\right)} \tag{A2}$$

$$PET_{PM}^s = \frac{\Delta(R_n - G) + (\rho_a C_p D - \Delta r_a^s (R_n - R_n^s))/(r_a^a + r_a^s)}{\lambda\left(\Delta + \gamma\left(1 + \frac{r_s^s}{r_a^a + r_a^s}\right)\right)} \tag{A3}$$

$$C_c = \frac{1}{1 + \frac{R_c R_a}{R_s (R_c + R_a)}} \tag{A4}$$

$$C_s = \frac{1}{1 + \frac{R_s R_a}{R_c (R_s + R_a)}} \tag{A5}$$

$$R_a = (\Delta + \gamma) r_a^a \tag{A6}$$

$$R_s = (\Delta + \gamma) r_a^s + \gamma r_s^s \tag{A7}$$

$$R_c = (\Delta + \gamma) r_a^c + \gamma r_s^c \tag{A8}$$

where many terms have been given by Eq.1-2, except

R_n^s = net radiation over soil surface = $R_n^s(1 - f_{veg}) = R_n^s \cdot \exp(-0.5 \cdot LAI)$

r_a^a = aerodynamic resistance between canopy height and reference level (s m^{-1})

r_s^s = surface resistance of the substrate (s m^{-1})

r_a^s = aerodynamic resistance between substrate and the canopy (s m^{-1})

r_s^c = bulk stomatal resistance of the canopy (s m^{-1})

r_a^c = bulk boundary layer resistance of the vegetative elements in the canopy (s m^{-1}).

In this study, the resistances are parameterized for the feasible minimal values based on the water-unlimited assumption for estimating PET. The substrate resistance r_s^s is set to zero s m^{-1} as a saturated surface. The canopy resistances are dependent on LAI (Shuttleworth and Wallace, 1985, Equations 19-20).

Deleted: Appendix A. Initial examination of PET methods and parameterizations
We conduct a preliminary analysis to identify the importance of surface characteristics. Each of the above processes are regarded as different options: (i) using active surface roughness or open water surface, (ii) seasonally varying or fixed surface conductance, and (iii) seasonally varying or fixed surface albedo.
Table A1 provides the PET methods and the parameters in the preliminary analysis. The first set of methods (a-d) are the existing physically-based PET approaches: the open-water Penman equation (OW), the FAO reference crop evapotranspiration for tall crop and short crop, and the Priestley-Taylor equation (PT).
Table A1. Summary of the PET methods with their ID, name and abbreviation code, and details about surface characteristics. ... [2]

Deleted: We examine seven algorithms (e-k) to isolate the effects of surface characteristics on PET. First, in methods (e), (f), (g), the aerodynamic conductance module is not active as we set Ga to the open water Ga_{ow}, indicating a smooth surface with low roughness (Equation 6). In methods (h), (i), (j), (k), we activate aerodynamic conductance using realistic surface roughness (Equation 9). Second, in methods (e), (i), (j), the surface conductance parameter is unconstrained as we set Gst_{max} to infinity. In methods (f), (g), (h), (k), we activate surface conductance using seasonal LAI dynamics and Gst_{max} from Kelliher et al. (1995). Lastly, in methods (f), (i), (k), the albedo parameter is not active as we set α to a constant (grass: 0.23, water: 0.08). In methods (e), (g), (h), (j), we activate albedo parameter using seasonal albedo dynamics.

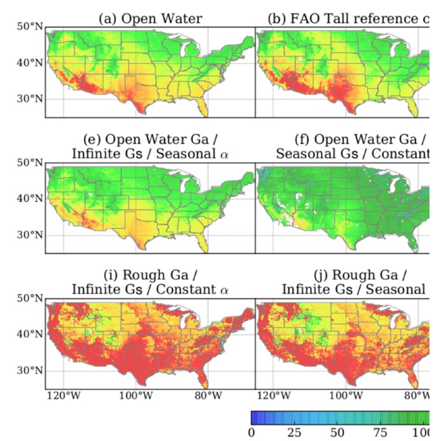

Figure A1. Growing season averages of AED derived from four PET methods and seven testing algorithms over the CONUS. Details and ID for each method are listed in Table A1.

Figure A1 displays the spatial patterns of growing season averages of these methods. For the classical Penman/Penman-Monteith methods (Fig. A1a-c), the highest mean growing season AED values are found in souther ... [3]

$$r_s^c = Rst \cdot \frac{1}{LAI_e} \qquad \text{(A9)}$$

$$r_a^c = r_b \cdot \frac{1}{2LAI} \qquad \text{(A10)}$$

Stomatal resistance Rst is set to Rst_{min} obtained by the land cover types in Table 1. The effective leaf area index LAI_e is LAI/2 and is capped to 2 (even when LAI is greater than 4). Note that, r_s^c does not have valid values for non-vegetated grid cells (at a specific time of the year or location). The leaf boundary layer resistance r_b is set to a value of 50 s m^{-1} (Brisson et al., 1998).

The formulas of aerodynamic resistances are given as follows (Shuttleworth and Gurney, 1990; Zhou et al., 2006).

$$r_a^s = \frac{h \cdot \exp(n) \ln\left(\frac{z_m - d_0}{z_0}\right)}{nk^2(h - d_0)} \left(\exp\left(-\frac{nz_{0g}}{h}\right) - \exp\left(-\frac{n(z_{0m} + d_p)}{h}\right)\right) \qquad \text{(A11)}$$

$$r_a^a = \frac{\ln\left(\frac{z_m - d_0}{z_0}\right) \ln\left(\frac{z_m - d_0}{h - d_0}\right)}{k^2 u_z} + \frac{\ln\left(\frac{z_m - d_0}{z_0}\right) h}{nk^2(h - d_0)} \left(\exp\left(n\left(1 - \frac{z_{0m} + d_p}{h}\right)\right) - 1\right) \qquad \text{(A12)}$$

where h is canopy height (m), k is the von Karman constant, z_{0m} is the "preferred" roughness length (m), $z_{0m} = h/8$, d_p is the "preferred" zero plane displacement height (m), $d_p = 0.63h$, z_{0g} is the roughness length of ground (m), u_z is the wind speed from the measurement height (m s^{-1}), and z_m is the measurement height (m), assuming $z_m = h + 2$.

d_0 is the zero plane displacement of canopy (m), n is the eddy diffusivity decay constant of the vegetation, and z_0 is the canopy roughness length (m). These terms are parameterized as following (Equations 22-26, Zhou et al., 2006):

$$n = \begin{cases} 2.5, & h \leq 1 \\ 2.306 + 0.194h, & 1 < h < 10 \\ 4.25, & h \geq 10 \end{cases} \qquad \text{(A13)}$$

$$d_0 = \begin{cases} h - z_{0c}/0.3, & LAI \geq 4 \\ 1.1h \cdot \ln\left(1 + (C_d LAI)^{0.25}\right), & LAI < 4 \end{cases} \qquad \text{(A14)}$$

$$z_0 = \min\left(0.3(h - d_0), z_{0g} + 0.3h(C_d LAI)^{0.5}\right) \qquad \text{(A15)}$$

$$C_d = \begin{cases} 1.4 \times 10^{-3}, & h = 0 \\ 0.25\left(-1 + \exp\left(0.909 - \frac{3.03z_{0c}}{h}\right)\right)^4, & h > 0 \end{cases} \qquad \text{(A16)}$$

$$z_{0c} = \begin{cases} 0.13h, & h \leq 1 \\ 0.139h - 0.009h^2, & 1 < h < 10 \\ 0.05h, & h \geq 10 \end{cases} \qquad \text{(A17)}$$

where z_{0c} is the roughness length for a closed canopy (m), C_d is the mean drag coefficient for individual leaves.

Code and data availability

The model codes are available online at https://github.com/pitcheverlasting (will become a public repo after acceptance).

The data generated in our study are published in this public repository: https://doi.org/10.6084/m9.figshare.12132696.v1. (active after acceptance).

The primary data and tools can be downloaded from the PRISM Climate Group at Oregon State University (http://www.prism.oregonstate.edu), the ESA CCI soil moisture project team (https://www.esa-soilmoisture-cci.org/node/145), the GIMMS LAI3g product team (https://drive.google.com/open?id=0BwL88nwumpqYaFJmR2poS0d1ZDQ), the Global Land Surface Satellite project (http://www.glass.umd.edu/Download.html), the SPEI R package released by Santiago Beguería and Sergio M. Vicente-Serrano at CSIC in Spain (https://cran.r-project.org/web/packages/SPEI/), the Global Land Cover Climatology project (https://archive.usgs.gov/archive/sites/landcover.usgs.gov/global_climatology.html), and the CDO software (https://code.zmaw.de/projects/cdo).

Author contributions

LP and JS conceived the idea, LP designed and implemented the PET experiments and analyzed the data. LP wrote the paper with contributions from ZW, ME, and EFW.

Competing interests

The authors declare that they have no conflict of interest.

Acknowledgements

This research has been supported by NASA under grant NNX14AB36A. We thank Dan Li at Boston University for the helpful discussions. We thank Philip Lu for proofreading.

References

Acreman, M. C., Harding, R. J., Lloyd, C. R., & McNeil, D. D. (2003). Evaporation characteristics of wetlands: experience from a wetgrassland and a reedbed using eddy correlation measurements. *Hydrology and Earth System Sciences*, *7*(1), 11–21. http://doi.org/10.5194/hess-7-11-2003

Allen, R. G., Pereira, L. S., Raes, D., & Smith, M. (1998). Crop evapotranspiration-Guidelines for computing crop water requirements-FAO Irrigation and drainage paper 56. *FAO*, *300*(9), D05109.

Allen, R. G., Walter, I. A., Elliott, R., Howell, T. A., Itenfisu, D., & Jensen, M. (2005). *The ASCE standardized reference evapotranspiration equation* (p. 4). Reston, VA 20191: American Society of Civil Engineers.

Andreadis, K. M., Clark, E. A., Wood, A. W., Hamlet, A. F., & Lettenmaier, D. P. (2005). Twentieth-Century Drought in the Conterminous United States. *Journal of Hydrometeorology*, *6*(6), 985–1001. https://doi.org/10.1175/jhm450.1

Andreadis, K. M., & Lettenmaier, D. P. (2006). Trends in 20th century drought over the continental United States. *Geophysical Research Letters*, *33*(10). https://doi.org/10.1029/2006gl025711

Barbeta, A., Ogaya, R., & Peñuelas, J. (2013). Dampening effects of long-term experimental drought on growth and mortality rates of a Holm oak forest. *Global Change Biology*, *19*(10), 3133–3144. https://doi.org/10.1111/gcb.12269

Beguería, S., Vicente-Serrano, S. M., Reig, F., & Latorre, B. (2013). Standardized precipitation evapotranspiration index (SPEI) revisited: parameter fitting evapotranspiration models, tools, datasets and drought monitoring. *International Journal of Climatology*, *34*(10), 3001–3023. https://doi.org/10.1002/joc.3887

Brisson, N., Itier, B., L'Hotel, J. C., & Lorendeau, J. Y. (1998). Parameterisation of the Shuttleworth-Wallace model to estimate daily maximum transpiration for use in crop models. *Ecological Modelling*, *107*(2-3), 159-169.

Broxton, P. D., Zeng, X., Sulla-Menashe, D., & Troch, P. A. (2014). A Global Land Cover Climatology Using MODIS Data. *Journal of Applied Meteorology and Climatology*, *53*(6), 1593–1605. https://doi.org/10.1175/jamc-d-13-0270.1

Brutsaert, W. (1982). The Surface Roughness Parameterization. In A. J. Davenport, B. B. Hicks, G. R. Hilst, R. E. Munn, & J. D. Smith (Eds.), *Evaporation into the Atmosphere* (pp. 113–127). Dordrecht: Springer Netherlands. https://doi.org/10.1007/978-94-017-1497-6_5

Brutsaert, W., & Stricker, H. (1979). An advection-aridity approach to estimate actual regional evapotranspiration. *Water Resources Research*, *15*(2), 443–450. https://doi.org/10.1029/wr015i002p00443

Campbell, G. S., & Norman, J. M. (1998). Wind. In *An introduction to environmental biophysics* (pp. 68-70). New York, NY: Springer.

Clark, J. S., Iverson, L., Woodall, C. W., Allen, C. D., Bell, D. M., Bragg, D. C., … Zimmermann, N. E. (2016). The impacts of increasing drought on forest dynamics structure, and biodiversity in the United States. *Global Change Biology*, *22*(7), 2329–2352. https://doi.org/10.1111/gcb.13160

Dai, A., Trenberth, K. E., & Qian, T. (2004). A Global Dataset of Palmer Drought Severity Index for 18702002: Relationship with Soil Moisture and Effects of Surface Warming. *Journal of Hydrometeorology*, *5*(6), 1117–1130. https://doi.org/10.1175/jhm-386.1

Daly, C., Halbleib, M., Smith, J. I., Gibson, W. P., Doggett, M. K., Taylor, G. H., … Pasteris, P. P. (2008). Physiographically sensitive mapping of climatological temperature and precipitation across the conterminous United States. *International Journal of Climatology*, *28*(15), 2031–2064. https://doi.org/10.1002/joc.1688

Daly, C., Neilson, R. P., & Phillips, D. L. (1994). A Statistical-Topographic Model for Mapping Climatological Precipitation over Mountainous Terrain. *Journal of Applied Meteorology*, *33*(2), 140–158. https://doi.org/10.1175/1520-0450(1994)033<0140:astmfm>2.0.co;2

Dewes, C. F., Rangwala, I., Barsugli, J. J., Hobbins, M. T., & Kumar, S. (2017). Drought risk assessment under climate change is sensitive to methodological choices for the estimation of evaporative demand. *Plos One*, *12*(3), e0174045. http://doi.org/10.1371/journal.pone.0174045

Dong, C., MacDonald, G. M., Willis, K., Gillespie, T. W., Okin, G. S., & Williams, A. P. (2019). Vegetation Responses to 20122016 Drought in Northern and Southern California. *Geophysical Research Letters*, *46*(7), 3810–3821. https://doi.org/10.1029/2019gl082137

Dorigo, W., Wagner, W., Albergel, C., Albrecht, F., Balsamo, G., Brocca, L., … Lecomte, P. (2017). ESA CCI Soil Moisture for improved Earth system understanding: State-of-the art and future directions. *Remote Sensing of Environment*, *203*, 185–215. https://doi.org/10.1016/j.rse.2017.07.001

Ek, M. B., Mitchell, K. E., Lin, Y., Rogers, E., Grunmann, P., Koren, V., et al. (2003). Implementation of Noah land surface model advances in the National Centers for Environmental Prediction operational mesoscale Eta model. *Journal of Geophysical Research*, *108*(D22), 2002JD003296. http://doi.org/10.1029/2002JD003296

Fang, L., Zhan, X., Hain, C. R., Yin, J., & Liu, J. (2018). Impact of GVF Derivation Methods on Noah Land Surface Model Simulations and WRF Model Forecasts. *Journal of Hydrometeorology*, *19*(12), 1917–1933. https://doi.org/10.1175/jhm-d-18-0075.1

Feng, S., Trnka, M., Hayes, M., & Zhang, Y. (2017). Why Do Different Drought Indices Show Distinct Future Drought Risk Outcomes in the U.S. Great Plains?. *Journal of Climate*, *30*(1), 265–278. https://doi.org/10.1175/jcli-d-15-0590.1

Forzieri, G., G Miralles, D., Ciais, P., Alkama, R., Ryu, Y., Duveiller, G., et al. (2020). Increased control of vegetation on global terrestrial energy fluxes. *Nature Climate Change*, *4*(2), 1–7. http://doi.org/10.1038/s41558-020-0717-0

Gruber, A., Dorigo, W. A., Crow, W., & Wagner, W. (2017). Triple collocation-based merging of satellite soil moisture retrievals. *IEEE Transactions on Geoscience and Remote Sensing*, *55*(12), 6780-6792. https://doi.org/10.1109/TGRS.2017.2734070.

Gruber, A., Scanlon, T., van der Schalie, R., Wagner, W., & Dorigo, W. (2019). Evolution of the ESA CCI Soil Moisture climate data records and their underlying merging methodology. *Earth System Science Data*, *11*, 717-739. https://doi.org/10.5194/essd-11-717-2019

Heim, R. R. (2002). A Review of Twentieth-Century Drought Indices Used in the United States. *Bulletin of the American Meteorological Society*, *83*(8), 1149–1166. https://doi.org/10.1175/1520-0477-83.8.1149

Hobbins, M. T., Wood, A., Streubel, D., & Werner, K. (2012). What Drives the Variability of Evaporative Demand across the Conterminous United States? *Journal of Hydrometeorology*, *13*(4), 1195–1214. http://doi.org/10.1175/JHM-D-11-0101.1

Hoerling, M., Eischeid, J., Kumar, A., Leung, R., Mariotti, A., Mo, K., … Seager, R. (2014). Causes and Predictability of the 2012 Great Plains Drought. *Bulletin of the American Meteorological Society*, *95*(2), 269–282. https://doi.org/10.1175/bams-d-13-00055.1

Katul, G. G., Oren, R., Manzoni, S., Higgins, C., & Parlange, M. B. (2012). Evapotranspiration: A process driving mass transport and energy exchange in the soil-plant-atmosphere-climate system. *Reviews of Geophysics*, *50*(3). https://doi.org/10.1029/2011rg000366

Kelliher, F. M., Leuning, R., Raupach, M. R., & Schulze, E.-D. (1995). Maximum conductances for evaporation from global vegetation types. *Agricultural and Forest Meteorology*, *73*(1-2), 1–16. https://doi.org/10.1016/0168-1923(94)02178-m

Kogan, F. N. (1995). Droughts of the Late 1980s in the United States as Derived from NOAA Polar-Orbiting Satellite Data. *Bulletin of the American Meteorological Society*, *76*(5), 655–668. https://doi.org/10.1175/1520-0477(1995)076<0655:dotlit>2.0.co;2

Kustas, W. P., Choudhury, B. J., Moran, M. S., Reginato, R. J., Jackson, R. D., Gay, L. W., & Weaver, H. L. (1989). Determination of sensible heat flux over sparse canopy using thermal infrared data. *Agricultural and Forest Meteorology*, *44*(3-4), 197–216. https://doi.org/10.1016/0168-1923(89)90017-8

Lang, N., Jetz, W., Schindler, K., & Wegner, J. D. (2023). A high-resolution canopy height model of the Earth. *Nature Ecology & Evolution*, *7*(11), 1778-1789.

Leuning, R., Zhang, Y. Q., Rajaud, A., Cleugh, H., & Tu, K. (2008). A simple surface conductance model to estimate regional evaporation using MODIS leaf area index and the Penman-Monteith equation. *Water Resources Research*, *44*(10), 1872. http://doi.org/10.1029/2007WR006562

Lhomme, J.-P., Troufleau, D., Monteny, B., Chehbouni, A., & Bauduin, S. (1997). Sensible heat flux and radiometric surface temperature over sparse Sahelian vegetation II. A model for the kB-1 parameter. *Journal of Hydrology*, *188-189*, 839–854. https://doi.org/10.1016/s0022-1694(96)03173-3

Liang, X., Lettenmaier, D. P., Wood, E. F., & Burges, S. J. (1994). A simple hydrologically based model of land surface water and energy fluxes for general circulation models. *Journal of Geophysical Research: Atmospheres (1984–2012)*, *99*(D7), 14415–14428. http://doi.org/10.1029/94JD00483

Liu, Q., Wang, L., Qu, Y., Liu, N., Liu, S., Tang, H., & Liang, S. (2013). Preliminary evaluation of the long-term GLASS albedo product. *International Journal of Digital Earth*, *6*(sup1), 69–95. https://doi.org/10.1080/17538947.2013.804601

Liu, Y. Y., Dorigo, W. A., Parinussa, R. M., de Jeu, R. A. M., Wagner, W., McCabe, M. F., … van Dijk, A. I. J. M. (2012). Trend-preserving blending of passive and active microwave soil moisture retrievals. *Remote Sensing of Environment*, *123*, 280–297. https://doi.org/10.1016/j.rse.2012.03.014

Loon, A. F. V. (2015). Hydrological drought explained. *Wiley Interdisciplinary Reviews: Water*, *2*(4), 359–392. https://doi.org/10.1002/wat2.1085

Lorenz, R., Davin, E. L., Lawrence, D. M., Stö Ckli, R., & Seneviratne, S. I. (2013). How important is vegetation phenology for European climate and heat waves? *Journal of Climate*, *26*(24), 10077–10100. http://doi.org/10.1175/JCLI-D-13-00040.1

Martens, B., Miralles, D. G., Lievens, H., van der Schalie, R., de Jeu, R. A. M., Fernández-Prieto, D., … Verhoest, N. E. C. (2017). GLEAM v3: satellite-based land evaporation and root-zone soil moisture. *Geoscientific Model Development*, *10*(5), 1903–1925. https://doi.org/10.5194/gmd-10-1903-2017

McDowell, N. G., Allen, C. D., Teixeira, K. A., Brando, P., Brienen, R., Chambers, J., et al. (2018). Drivers and mechanisms of tree mortality in moist tropical forests. *New Phytologist*, *219*(3), 851–869. http://doi.org/10.1111/nph.15027

McKee, T. B., Doesken, N. J., Kleist, J., & others. (1993). The relationship of drought frequency and duration to time scales. In *Proceedings of the 8th Conference on Applied Climatology* (Vol. 17, pp. 179–183). Boston, MA: American Meteorological Society.

Monteith, J. L. (1965). Evaporation and environment. *Symposia of the Society for Experimental Biology*, *19*, 205–234.

Monteith, J., & Unsworth, M. (2013). Micrometeorology. In *Principles of environmental physics: plants, animals, and the atmosphere* (pp. 301-310). Academic Press.

Moran, M. S., Rahman, A. F., Washburne, J. C., Goodrich, D. C., Weltz, M. A., & Kustas, W. P. (1996). Combining the Penman-Monteith equation with measurements of surface temperature and reflectance to estimate evaporation rates of semiarid grassland. *Agricultural and Forest Meteorology*, *80*(2-4), 87–109. http://doi.org/10.1016/0168-1923(95)02292-9

Nadeau, D. F., Brutsaert, W., Parlange, M. B., Bou-Zeid, E., Barrenetxea, G., Couach, O., … Vetterli, M. (2009). Estimation of urban sensible heat flux using a dense wireless network of observations. *Environmental Fluid Mechanics*, *9*(6), 635–653. https://doi.org/10.1007/s10652-009-9150-7

Norman, J. M., Kustas, W. P., & Humes, K. S. (1995). Source approach for estimating soil and vegetation energy fluxes in observations of directional radiometric surface temperature. *Agricultural and Forest Meteorology*, *77*(3-4), 263–293. https://doi.org/10.1016/0168-1923(95)02265-y

Or, D., & Lehmann, P. (2019). Surface Evaporative Capacitance: How Soil Type and Rainfall Characteristics Affect Global-Scale Surface Evaporation. *Water Resources Research*, *55*(1), 519–539. https://doi.org/10.1029/2018wr024050

Palmer, W. C. (1965). *Meteorological drought* (Vol. Research paper No. 45, p. 58). Washington, DC: U.S. Weather Bureau.

Paulo, A. A., Rosa, R. D., & Pereira, L. S. (2012). Climate trends and behaviour of drought indices based on precipitation and evapotranspiration in Portugal. *Natural Hazards and Earth System Sciences*, *12*(5), 1481–1491. https://doi.org/10.5194/nhess-12-1481-2012

Pederson, N., Bell, A. R., Knight, T. A., Leland, C., Malcomb, N., Anchukaitis, K. J., … Riddle, J. (2012). A long-term perspective on a modern drought in the American Southeast. *Environmental Research Letters*, *7*(1), 014034. https://doi.org/10.1088/1748-9326/7/1/014034

Peng, L., Li, D., & Sheffield, J. (2018). Drivers of Variability in Atmospheric Evaporative Demand: Multiscale Spectral Analysis Based on Observations and Physically Based Modeling. *Water Resources Research*, *54*(5), 3510–3529. http://doi.org/10.1029/2017WR022104

Peng, L., Zeng, Z., Wei, Z., Chen, A., Wood, E. F., & Sheffield, J. (2019). Determinants of the ratio of actual to potential evapotranspiration. *Global change biology*, *25*(4), 1326-1343. https://doi.org/10.1111/gcb.14577

Penman, H. L. (1948). Natural evaporation from open water, bare soil and grass. *Proceedings of the Royal Society of London Series A*, *193*, 120–145.

Peters, M. P., Iverson, L. R., & Matthews, S. N. (2014). *Spatio-temporal trends of drought by forest type in the conterminous United States, 1960-2013*. U.S. Department of Agriculture Forest Service, Northern Research Station. https://doi.org/10.2737/nrs-rmap-7

Piao, S., Zhang, X., Chen, A., Liu, Q., Lian, X., Wang, X., ... & Wu, X. (2019). The impacts of climate extremes on the terrestrial carbon cycle: A review. *Science China Earth Sciences*, *62*, 1551-1563. https://link.springer.com/article/10.1007/s11430-018-9363-5

Potop, V. (2011). Evolution of drought severity and its impact on corn in the Republic of Moldova. *Theoretical and Applied Climatology*, *105*(3-4), 469–483. https://doi.org/10.1007/s00704-011-0403-2

Potop, V., Možný, M., & Soukup, J. (2012). Drought evolution at various time scales in the lowland regions and their impact on vegetable crops in the Czech Republic. *Agricultural and Forest Meteorology*, *156*, 121–133. https://doi.org/10.1016/j.agrformet.2012.01.002

Priestley, C. H. B., & Taylor, R. J. (1972). On the assessment of surface heat flux and evaporation using large-scale parameters. *Monthly Weather Review*, *100*(2), 81–92.

Qu, Y., Liu, Q., Liang, S., Wang, L., Liu, N., & Liu, S. (2014). Direct-Estimation Algorithm for Mapping Daily Land-Surface Broadband Albedo From MODIS Data. *IEEE Transactions on Geoscience and Remote Sensing*, *52*(2), 907–919. https://doi.org/10.1109/tgrs.2013.2245670

Rigden, A., Li, D., & Salvucci, G. (2018). Dependence of thermal roughness length on friction velocity across land cover types: A synthesis analysis using AmeriFlux data. *Agricultural and Forest Meteorology*, *249*, 512–519. https://doi.org/10.1016/j.agrformet.2017.06.003

Ross, T., & Lott, N. (2003). A climatology of 1980-2003 extreme weather and climate events. *National Climatic Data Center Technical Report*, *1*, 14.

Seager, R., Tzanova, A., & Nakamura, J. (2009). Drought in the Southeastern United States: Causes Variability over the Last Millennium, and the Potential for Future Hydroclimate Change. *Journal of Climate*, *22*(19), 5021–5045. https://doi.org/10.1175/2009jcli2683.1

Sellers, P. J., Randall, D. A., Collatz, G. J., Berry, J. A., Field, C. B., Dazlich, D. A., et al. (1996). A revised land surface parameterization (SiB2) for atmospheric GCMs .1. Model formulation, *9*(4), 676–705.

Seneviratne, S. I., Corti, T., Davin, E. L., Hirschi, M., Jaeger, E. B., Lehner, I., et al. (2010). Investigating soil moisture–climate interactions in a changing climate: A review. *Earth-Science Reviews*, *99*(3-4), 125–161. http://doi.org/10.1016/j.earscirev.2010.02.004

Seneviratne, S. I. (2012). Historical drought trends revisited. *Nature*, *491*(7424), 338–339. http://doi.org/10.1038/491338a

Sheffield, J., & Wood, E. F. (2007). Characteristics of global and regional drought, 1950–2000: Analysis of soil moisture data from off-line simulation of the terrestrial hydrologic cycle. *Journal of Geophysical Research: Atmospheres (1984–2012)*, *112*(D17), D17115. http://doi.org/10.1029/2006JD008288

Sheffield, J., Wood, E. F., & Roderick, M. L. (2012). Little change in global drought over the past 60 years. *Nature*, *491*(7424), 435–438. https://doi.org/10.1038/nature11575

Shuttleworth, W. J., & Wallace, J. S. (1985). Evaporation from sparse crops-an energy combination theory. *Quarterly Journal of the Royal Meteorological Society*, *111*(469), 839-855.

Shuttleworth, W. J., & Gurney, R. J. (1990). The theoretical relationship between foliage temperature and canopy resistance in sparse crops. *Quarterly Journal of the Royal Meteorological Society*, *116*(492), 497-519.

Shuttleworth, W. J. (1993). Chapter 4 Evaporation. In D. R. Maidment (Ed.), *Handbook of hydrology* (Vol. 9780070). Sydney: McGraw-Hill.

Simard, M., Pinto, N., Fisher, J. B., & Baccini, A. (2011). Mapping forest canopy height globally with spaceborne lidar. *Journal of Geophysical Research: Biogeosciences*, *116*(G4). https://doi.org/10.1029/2011JG001708

Stewart, J. B., Kustas, W. P., Humes, K. S., Nichols, W. D., Moran, M. S., & de Bruin, H. A. R. (1994). Sensible Heat Flux-Radiometric Surface Temperature Relationship for Eight Semiarid Areas. *Journal of Applied Meteorology*, *33*(9), 1110–1117. https://doi.org/10.1175/1520-0450(1994)033<1110:shfrst>2.0.co;2

Sun, S., Bi, Z., Xiao, J., Liu, Y., Sun, G., Ju, W., ... & Chen, H. (2023). A global 5 km monthly potential evapotranspiration dataset (1982–2015) estimated by the Shuttleworth–Wallace model. *Earth System Science Data*, *15*(11), 4849-4876.

Thornthwaite, C. W. (1948). An Approach toward a Rational Classification of Climate. *Geographical Review*, 38(1):55.

Trenberth, K. E., Dai, A., van der Schrier, G., Jones, P. D., Barichivich, J., Briffa, K. R., & Sheffield, J. (2013). Global warming and changes in drought. *Nature Climate Change*, *4*(1), 17–22. https://doi.org/10.1038/nclimate2067

Troufleau, D., Lhomme, J. P., Monteny, B., & Vidal, A. (1997). Sensible heat flux and radiometric surface temperature over sparse Sahelian vegetation. I. An experimental analysis of the kB-1 parameter. *Journal of Hydrology*, *188-189*, 815–838. https://doi.org/10.1016/s0022-1694(96)03172-1

Verhoef, A., Bruin, H. A. R. D., & Hurk, B. J. J. M. V. D. (1997). Some Practical Notes on the Parameter kB-1 for Sparse Vegetation. *Journal of Applied Meteorology*, *36*(5), 560–572. https://doi.org/10.1175/1520-0450(1997)036<0560:spnotp>2.0.co;2

Verma, S. B. (1989). Aerodynamic resistances to transfers of heat, mass and momentum. In: Black, T. A., Spittlehouse, D. L., Novak, M. D., Price, D. T. (Eds.), *Estimation of Areal Evapotranspiration* (pp. 13-20). IAHS Press.

Vicente-Serrano, S. M., Beguería, S., Lorenzo-Lacruz, J., Camarero, J. J., López-Moreno, J. I., Azorin-Molina, C., … Sanchez-Lorenzo, A. (2012). Performance of Drought Indices for Ecological Agricultural, and Hydrological Applications. *Earth Interactions*, *16*(10), 1–27. https://doi.org/10.1175/2012ei000434.1

Vicente-Serrano, S. M., Beguería, S., & López-Moreno, J. I. (2010). A Multiscalar Drought Index Sensitive to Global Warming: The Standardized Precipitation Evapotranspiration Index. *Journal of Climate*, *23*(7), 1696–1718. https://doi.org/10.1175/2009jcli2909.1

Vicente-Serrano, S. M., Gouveia, C., Camarero, J. J., Begueria, S., Trigo, R., Lopez-Moreno, J. I., … Sanchez-Lorenzo, A. (2013). Response of vegetation to drought time-scales across global land biomes. *Proceedings of the National Academy of Sciences*, *110*(1), 52–57. https://doi.org/10.1073/pnas.1207068110

Vicente-Serrano, S. M., der Schrier, G. V., Beguería, S., Azorin-Molina, C., & Lopez-Moreno, J.-I. (2015). Contribution of precipitation and reference evapotranspiration to drought indices under different climates. *Journal of Hydrology*, *526*, 42–54. https://doi.org/10.1016/j.jhydrol.2014.11.025

Wei, Z., Yoshimura, K., Wang, L., G Miralles, D., Jasechko, S., & Lee, X. (2017). Revisiting the contribution of transpiration to global terrestrial evapotranspiration. *Geophysical Research Letters*, *44*(6), 2792–2801. http://doi.org/10.1002/2016GL072235

Wilhite, D. A. (2000), Drought as a natural hazard: Concepts and definitions, In *Drought: A Global Assessment* (pp. 3-18). London: Routledge.

Wilhite, D. A., Sivakumar, M. V. K., & Pulwarty, R. (2014). Managing drought risk in a changing climate: The role of national drought policy. *Weather and Climate Extremes*, *3*, 4–13. https://doi.org/10.1016/j.wace.2014.01.002

Williams, A. P., Allen, C. D., Macalady, A. K., Griffin, D., Woodhouse, C. A., Meko, D. M., et al. (2012). Temperature as a potent driver of regional forest drought stress and tree mortality. *Nature Climate Change*, *3*(3), 292–297. http://doi.org/10.1038/nclimate1693

Xia, Y., Mitchell, K., Ek, M., Sheffield, J., Cosgrove, B., Wood, E., … Mocko, D. (2012). Continental-scale water and energy flux analysis and validation for the North American Land Data Assimilation System project phase 2 (NLDAS-2): 1. Intercomparison and application of model products. *Journal of Geophysical Research: Atmospheres*, *117*(D3), n/a–n/a. https://doi.org/10.1029/2011jd016048

Xu, H., Lian, X., Slette, I. J., Yang, H., Zhang, Y., Chen, A., & Piao, S. (2022). Rising ecosystem water demand exacerbates the lengthening of tropical dry seasons. *Nature Communications*, *13*(1), 4093. https://www.nature.com/articles/s41467-022-31826-y

Yang, H., Munson, S. M., Huntingford, C., Carvalhais, N., Knapp, A. K., Li, X., ... & Chen, A. (2023). The detection and attribution of extreme reductions in vegetation growth across the global land surface. *Global Change Biology*, *29*(8), 2351-2362. https://onlinelibrary.wiley.com/doi/full/10.1111/gcb.16595

Yan, H., Wang, S. Q., Billesbach, D., Oechel, W., Zhang, J. H., Meyers, T., … Scott, R. (2012). Global estimation of evapotranspiration using a leaf area index-based surface energy and water balance model. *Remote Sensing of Environment*, *124*, 581–595. https://doi.org/10.1016/j.rse.2012.06.004

Yang, K., Koike, T., Ishikawa, H., Kim, J., Li, X., Liu, H., … Wang, J. (2008). Turbulent Flux Transfer over Bare-Soil Surfaces: Characteristics and Parameterization. *Journal of Applied Meteorology and Climatology*, *47*(1), 276–290. https://doi.org/10.1175/2007jamc1547.1

Yang, R., & Friedl, M. A. (2003). Determination of Roughness Lengths for Heat and Momentum Over Boreal Forests. *Boundary-Layer Meteorology*, *107*(3), 581–603. https://doi.org/10.1023/a:1022880530523

Yang, Y., Roderick, M. L., Zhang, S., McVicar, T. R., & Donohue, R. J. (2019). Hydrologic implications of vegetation response to elevated CO2 in climate projections. *Nature Climate Change*, *9*(1), 44–48. https://doi.org/10.1038/s41558-018-0361-0

Zhang, L., Jiao, W., Zhang, H., Huang, C., & Tong, Q. (2017). Studying drought phenomena in the Continental United States in 2011 and 2012 using various drought indices. *Remote Sensing of Environment*, *190*, 96–106. https://doi.org/10.1016/j.rse.2016.12.010

Zhao, H., Gao, G., An, W., Zou, X., Li, H., & Hou, M. (2017). Timescale differences between SC-PDSI and SPEI for drought monitoring in China. *Physics and Chemistry of the Earth Parts A/B/C*, *102*, 48–58. https://doi.org/10.1016/j.pce.2015.10.022

Zhou, M. C., Ishidaira, H., Hapuarachchi, H. P., Magome, J., Kiem, A. S., & Takeuchi, K. (2006). Estimating potential evapotranspiration using Shuttleworth–Wallace model and NOAA-AVHRR NDVI data to feed a distributed hydrological model over the Mekong River basin. *Journal of Hydrology*, 327(1-2), 151-173. https://doi.org/10.1016/j.jhydrol.2005.11.013

Zhu, Z., Bi, J., Pan, Y., Ganguly, S., Anav, A., Xu, L., … Myneni, R. (2013). Global Data Sets of Vegetation Leaf Area Index (LAI)3g and Fraction of Photosynthetically Active Radiation (FPAR)3g Derived from Global Inventory Modeling and Mapping Studies (GIMMS) Normalized Difference Vegetation Index (NDVI3g) for the Period 1981 to 2011. *Remote Sensing*, *5*(2), 927–948. https://doi.org/10.3390/rs5020927

Zilitinkevich, S. S., Grachev, A. A., & Fairall, C. W. (2001). Scaling Reasoning and Field Data on the Sea Surface Roughness Lengths for Scalars. *Journal of the Atmospheric Sciences*, *58*(3), 320–325. https://doi.org/10.1175/1520-0469(2001)058<0320:nacraf>2.0.co;2

Page 6: [1] Deleted **Liqing Peng** **2/7/24 12:58:00 PM**

Page 26: [2] Deleted **Liqing Peng** **2/11/24 6:31:00 PM**

Page 26: [3] Deleted **Liqing Peng** **2/11/24 6:31:00 PM**